Analytic Rate Theory of Polariton Relaxation that Explains Long Polariton Lifetime

Yifan Lai,[1, a)] Wenxiang Ying,[1] Todd D. Krauss,[1, 2, 3] and Pengfei Huo[1, 2, 3, b)]
[1)] *Department of Chemistry, University of Rochester, 120 Trustee Road, Rochester, New York 14627, U.S.A.*
[2)] *The Institute of Optics, Hajim School of Engineering, University of Rochester, Rochester, New York 14627, U.S.A.*
[3)] *Center for Coherence and Quantum Science, University of Rochester, Rochester, New York 14627, USA*

Hybridization of a molecular exciton with a quantized photon creates a polariton. Despite extensive experimental investigations, the apparent lifetime of the exciton-polariton is not well understood. We examined the steady-state population dynamics for a Holstein-Tavis-Cumming Hamiltonian to illuminate the long-term polaritonic dynamics and lifetime of the exciton polariton in an optical cavity. For a realistic description of polariton relaxation, cavity loss and various exciton decay channels are included in the model. We found that in the presence of weak but finite exciton loss, the apparent lifetime of the lower polariton coincides with the out-of-cavity exciton lifetime and is independent of cavity-matter detuning. This is a simple explanation for the experimentally observed lifetimes for exciton polaritons, and theoretically justifies the dark state reservoir hypothesis. Further, if the upper polariton is initially populated, the system reaches the steady state very quickly, leading to single-exponential polariton relaxation. Starting from the lower polariton leads to a longer pre-steady-state time period, leading to double-exponential relaxation. Finally, we considered the effect of site orientational disorders and the exciton frequency disorderers. Under the collective limit, the effects of this disorder can be included in Fermi's golden rule population dynamics without explicit sampling. For the exciton energy disorders, numerical calculations are needed. Our theoretical framework is applicable to interpret exciton-polariton experiments, especially related to the measured apparent lifetime of polaritons.

I. INTRODUCTION

The strong collective coupling between molecular excitations to confined photon modes inside an optical cavity generate excitonic polaritons.[1–3] These quantum superpositions are hybrid states of light and matter, and their formation and subsequent dynamics are believed to be integral to various interesting phenomena, including cavity-induced modification of photo-chemical reactivity[4–10], enhanced transport of delocalized excitons[11–21], room temperature Bose-Einstein condensates with laser pumping[22–24], and as a qubit candidate for quantum information applications[25,26]. It was also believed that vibrational polariton played a central role in understanding vibrational strong coupling (VSC)-induced chemical reactivities[27–36], cautions are needed to make the same claim as VSC could be in a different regime compared to the exciton strong coupling (ESC) regime.

As polaritons are central to strong light-matter coupling phenomena and potential applications to photophysics and photochemistry, the lifetime of the polariton during population dynamics has been the subject of experimental study, commonly through transient pump-probe spectroscopy[37–41], linewidth measurement[42,43] or direct population probing such as photon counting[44–48], as well as theoretical simulation. The most intuitive analysis may conclude that the polariton relaxation rate should be a combination of the loss rates of cavity Γ_c and the exciton loss rate Γ_x, weighed by their respective Hopfield coefficient, plus a small correction term for the population transfer between polariton and dark states, expressed as follows[49]

$$\frac{1}{\tau_\pm} = \left|\langle \pm|\mathrm{G},1\rangle\right|^2 \Gamma_c + \left(1 - \left|\langle \pm|\mathrm{G},1\rangle\right|^2\right)\Gamma_{ex} + \gamma(k_{\pm\leftrightarrow\mathcal{D}}), \tag{1}$$

where $\tau_\pm$ is the lifetime for polariton states $|\pm\rangle$, Γ_c is the cavity loss rate, Γ_{ex} is the exciton loss rate, γ is a rate characterize the transition from polariton states $|\pm\rangle$ to the dark states manifold $\{|\mathcal{D}\rangle\}$, and $|\mathrm{G},1\rangle \equiv |\mathrm{G}\rangle \otimes |1\rangle$ represents the 1-photon dressed molecular ground states.

Several experimental studies that measure excitonic polariton relaxation suggest that the polariton lifetimes are typically much longer (often by several orders of magnitude) than the cavity loss timescale, with no apparent detuning dependency.[37,39,49–53] or weak detuning dependency[45]. Various theoretical explanations have been proposed for this unexpectedly long lifetime, including long-timescale non-Markovian dynamics[9], interaction with intermediate states[54], and dark states acting as a population reservoir for the polariton,[52] prolonging their observed lifetime. In this study, we analyze the steady-state polaritonic population dynamics to demonstrate a *simple*, *quantitative* explanation for these long-lived, detuning-independent polariton lifetimes and the corresponding parameter range for this phenomenon.

Given the inherent collective nature of the polaritons, as well as other related collective optical phenomena such as Dicke superradiance emission[55–57], the effect of potentially symmetry-breaking disorder of the sites has been the focus of recent theoretical works.[58–65] The most

[a)] Electronic mail: ylai19@ur.rochester.edu
[b)] Electronic mail: pengfei.huo@rochester.edu

straightforward way to simulate the effect of disorder on polaritonic dynamics is to sample each site's energy, orientation, and positions explicitly, followed by performing an average over the simulated dynamics of the samples. Existing computational methods capable of such simulation at a collective scale (number of sites $N \geq 10^6$) include collective dynamics using truncated equations CUT-E[66–68], and trajectory-based methods accelerated via sparsity.[69–71] However, a more application-friendly theoretical treatment of site disorder would eliminate explicit sampling and include the effects of the disorder as a set of parameters, such as a reduction in Rabi splitting or collective relaxation.

In the present work, we study the highly collective excitonic polariton dynamics via Fermi's golden rule (FGR)[72]. We develop a theoretical explanation for the apparent contradiction between long, detuning-independent polariton lifetimes and fast, detuning-dependent cavity loss via the steady-state dynamics of lower polariton (LP) and the dark state manifold. Three channels of Lindbladian loss, local, collective (superradiant), and cavity loss are considered for a comprehensive description of the relaxation process. Elementary expressions for the polariton lifetime and the timescale corresponding to the steady state are derived under appropriate and realistic parameter ranges. Additionally, we showed that the effect of isotropic orientational disorder of the sites, despite its symmetry-breaking characteristics, can be handled within the framework of FGR without explicit sampling of the site angles. The effect of such disorder comes in the form of corrections to Rabi splitting, population transfer rates, and Lindbladian loss, which are calculated in closed form.

II. THEORY

Here, we develop an analytic theory to explain the often experimentally observed long lifetime of polaritons. We quickly review the FGR expressions in Sec. II A, the Lindblad operators we used to describe cavity loss and exciton decay in Sec. II B, and use this framework to derive the main results of this work in Sec. II C-II D. The main theoretical resutls are: (1) the apparent lifetime of the steady-state (Eq. 30, and Eq. 28 for the exact form), (2) the time scale for the initially excited polariton system to appraoching to this SS behavior (Eq. 34), and (3) the FGR rates when considering the dipole orientational disorders (Eq. 47).

A. Fermi's Golden Rule Rates for Polariton Dynamics

We consider a collection of N two-level systems (which can be either electronic or vibrational excitations of molecules), referred to as *sites*, inside and coupled to a cavity. It is described by the Holstein-Tavis-Cummings (HTC) model in the single exciton basis[62,73–75]

$$\begin{aligned}\hat{H} = \hbar\omega_{\mathrm{x}} \sum_{n=0}^{N-1} |n\rangle\langle n| + \hbar\omega_{\mathrm{c}} |\mathrm{G},1\rangle\langle \mathrm{G},1| + \hat{H}_{\mathrm{b}} + \hat{H}_{\mathrm{sb}} \\ +\hbar g_{\mathrm{c}} \sum_{n=0}^{N-1} \Big(|\mathrm{G},1\rangle\langle n| + |n\rangle\langle \mathrm{G},1| \Big).\end{aligned} \tag{2}$$

Here, $\hbar\omega_{\mathrm{x}}$ is the site exciton energy, $n \in \{0, 1 \cdots N-1\}$ is the site index, $|n\rangle \equiv |n,0\rangle \equiv |e_n\rangle \otimes |0\rangle$ and $|\mathrm{G},1\rangle \equiv |G\rangle \otimes |1\rangle$ is the single-site excited state of site n and the single photon state, respectively, ω_{c} is the photon frequency, and g_{c} is the single molecule light-matter coupling strength. Experimentally, $N \approx 10^6 - 10^{12}$ was estimated as the number of molecules coupled to a cavity mode in VSC regime[76–79] as well as electronic coupling regime, although the recent experiments[80] of spectroscopy and transport dynamics in VSC suggests that $N \approx 10^3 - 10^4$. For CdSe NPL coupled to the cavity under the excitonic strong coupling regime, it was estimated that $N \approx 10^3 - 10^5$ due to the large transition dipole of the NPL.[45,75] In this work, we will focus on the collective coupling parameter range and analyze the effect of N on polariton lifetime, with the range of $N \approx 10^6$.

It is well known that the polaritonic dynamics depend strongly on the phonon environment.[81] In this model described by Eq. 2, each site is coupled to its local phonon environment, which is modeled by $\hat{H}_{\mathrm{b}} + \hat{H}_{\mathrm{sb}}$. All baths are assumed to be harmonic and identical for all sites n, expressed as follows

$$\hat{H}_{\mathrm{b}} = \sum_n \sum_a \hbar\omega_a \hat{b}^\dagger_{a,n} \hat{b}_{a,n} \tag{3a}$$

$$\hat{H}_{\mathrm{sb}} = \sum_n |n\rangle\langle n| \otimes \sum_a c_a \Big(\hat{b}^\dagger_{a,n} + \hat{b}_{a,n} \Big), \tag{3b}$$

where a is the bath mode index, and $\hat{b}^\dagger_{a,n}$ are the raising operate for the a_{th} harmonic bath mode of the n_{th} site, with frequency ω_a. The exciton-phonon coupling is characterized by the spectral density defined as[82]

$$J(\omega) = \pi\hbar^{-1} \sum_a c_a^2 \delta(\omega - \omega_a). \tag{4}$$

In the current study, we refer to the electronic and the photonic DOFs as the *system* DOFs, leaving everything else (phonons) as the *bath* DOFs.

Dynamics simulation via the quantum master equation (QME) approaches[72] (including FGR) requires casting the system Hamiltonian into its eigenbasis. We transform the real-space Hamiltonian Eq. 2 into a reciprocal space polaritonic basis.[33,83,84] The basis includes $N-1$ dark states

$$|D_j\rangle = \frac{1}{\sqrt{N}} \sum_{n=0}^{N-1} \exp(-2\pi i \, \frac{nj}{N}) \, |n\rangle \tag{5}$$

for $j \in \{1, 2, \cdots, N-1\}$, which are delocalized (span over all exciton states) and optically dark when there is

no disorders. The optically bright state is $j = 0$ special case of Eq. 5,

$$|B\rangle \equiv |j = 0\rangle = \frac{1}{\sqrt{N}} \sum_{n=0}^{N-1} |n\rangle \tag{6}$$

To differentiate between the site (real-space) basis and the reciprocal basis, $\{m, n, \cdots\}$ will be used to index the site basis, and $\{j, k, \cdots\}$ will be used to index the reciprocal basis. The polariton states are mixtures of the photon state and the optically bright $j = 0$ state,

$$|+\rangle = \sin\phi \ |\mathrm{G}, 1\rangle + \cos\phi \ \frac{1}{\sqrt{N}} \sum_{n=0}^{N-1} |n\rangle \tag{7a}$$

$$|-\rangle = \cos\phi \ |\mathrm{G}, 1\rangle - \sin\phi \ \frac{1}{\sqrt{N}} \sum_{n=0}^{N-1} |n\rangle \tag{7b}$$

with the mixing angle ϕ as

$$\phi = \frac{1}{2} \tan^{-1} \left(\frac{2\sqrt{N} g_\mathrm{c}}{\omega_\mathrm{x} - \omega_\mathrm{c}} \right) \in [0, \frac{\pi}{2}). \tag{8}$$

The above polariton states $|\pm\rangle$ and dark states $\mathcal{D} \equiv \{|D_j\rangle\}$ are the eigenstes of the polariton Hamiltonian (system Hamiltonian)

$$\begin{aligned} \hat{H}_\mathrm{s} &\equiv \hat{H} - \hat{H}_\mathrm{b} - \hat{H}_\mathrm{sb} \\ &= \hbar\omega_+ |+\rangle\langle+| + \hbar\omega_- |-\rangle\langle-| + \sum_{j=1}^{N-1} \hbar\omega_\mathrm{x} |D_j\rangle\langle D_j| \,, \end{aligned} \tag{9}$$

and the energy of the polaritons as

$$\omega_\pm = \frac{\omega_\mathrm{x} + \omega_\mathrm{c}}{2} \pm \frac{1}{2} \sqrt{4N g_\mathrm{c}^2 + (\omega_\mathrm{x} - \omega_\mathrm{c})^2}. \tag{10}$$

The readers may refer to Ref. 72 for derivation details and explicit expressions of the Hamiltonian in Eq. 2 in the polaritonic basis (see Eq. A2 in Appendix A of Ref. 72).

The population dynamics governed by the polaritonic HTC Hamiltonian is described by non-equilibrium Fermi's golden rule (NE-FGR)[85,86] and equilibrium Fermi's golden rule (E-FGR). FGR is a perturbative theory based on treating the off-diagonal elements of the Hamiltonian as a perturbation, which in the polariton and dark states basis assumes weak system-bath coupling (exciton-phonon coupling). We expect this assumption to be valid in the collective limit $N \approx 10^6 \sim 10^{12}$, since all off-diagonal exciton-phonon coupling terms scale with $1/\sqrt{N}$.

Following the existing time-domain derivation for population quantum master equation (QME),[85–88], the FGR population equation of motion (EOM) is

$$\frac{\mathrm{d}}{\mathrm{d}t} P_J(t) = \sum_{I \neq J} k_{I\to J}(t) P_I(t) - \sum_{F \neq J} k_{J\to F}(t) P_J(t) \tag{11}$$

where the time-dependent rates are the Fourier transform of the correlation functions, the time-independent E-FGR rates are taken at the limit $t \to \infty$.

$$k_{I\to F}(t) = \frac{2}{\hbar^2} \mathrm{Re} \int_0^t \mathrm{d}s \ C_{I\to F}(t, s) \tag{12}$$

Following our previous application of FGR to cavity polaritons,[72] we combine the $N - 1$ dark mode populations into one overall dark state population $P_\mathcal{D} = \sum_{j=1}^{N-1} P_j$. Therefore, the EOM Eq. 11 concerns the populations of three states $I, F \in \{+, -, \mathcal{D}\}$. In the collective limit, the relevant correlation functions are t-independent, $C_{I\to F}(t, s) \to C_{I\to F}(s)$ and differ only by the FF frequency and a prefactor

$$C_{\pm\to\mathcal{D}}(s) = e^{i(\omega_\pm - \omega_\mathrm{x})s} \ \frac{N-1}{2}(1 \pm \cos 2\phi) \ C_{\mathcal{D}\to\mathcal{D}}(s) \tag{13a}$$

$$C_{\mathcal{D}\to\pm}(s) = e^{i(\omega_\mathrm{x} - \omega_\pm)s} \ \frac{1}{2}(1 \pm \cos 2\phi) \ C_{\mathcal{D}\to\mathcal{D}}(s) \tag{13b}$$

$$C_{\pm\to\mp}(s) = e^{i(\omega_\pm - \omega_\mp)s} \ \frac{1}{4} \sin^2 2\phi \ C_{\mathcal{D}\to\mathcal{D}}(s) \tag{13c}$$

where the common dark-to-dark correlation function $C_{\mathcal{D}\to\mathcal{D}}(s)$ is expressed as

$$\begin{aligned} C_{\mathcal{D}\to\mathcal{D}}(s) &= \frac{\hbar}{N\pi} \int_0^\infty \mathrm{d}\omega J(\omega) \Big[\coth \frac{\beta\hbar\omega}{2} \cos\omega s + i \sin\omega s \Big] \\ &= \frac{2}{N\beta} \gamma_\beta(s) + \frac{i\hbar}{N} \dot{\gamma}(s), \end{aligned} \tag{14}$$

where the definition for the frictions kernel γ_β is adopted from our previous work,[72]

$$\gamma_\beta(s) = \frac{\beta\hbar}{2\pi} \int_0^\infty \mathrm{d}\omega \ J(\omega) \cdot \coth \left(\frac{1}{2} \beta\hbar\omega \right) \cos(\omega s) \tag{15a}$$

$$\gamma(s) = \gamma_{\beta=0}(s) = \frac{1}{\pi} \int_0^\infty \mathrm{d}\omega \ \frac{J(\omega)}{\omega} \cos(\omega s) \tag{15b}$$

$$\dot{\gamma}(s) = \frac{1}{\pi} \int_0^\infty \mathrm{d}\omega \ J(\omega) \cdot \sin(\omega s), \tag{15c}$$

The NE-FGR rate constant is thus $k_{I\to F}(t) = \frac{2}{\hbar^2} \mathrm{Re} \int_0^t \mathrm{d}s \ C_{I\to F}(s)$. Under the equilibrium limit ($t \to \infty$ in Eq. 11 using Eq. 13), the rate constant $k_{I\to F} \equiv k_{I\to F}$ can be evaluated in close form, yielding the well-known E-FGR rate expressions

$$k_{\pm\to\mathcal{D}} = \frac{N-1}{N\hbar}(1 \pm \cos 2\phi) \frac{J(|\omega_\pm - \omega_\mathrm{x}|)}{\left|1 - e^{-\beta\hbar(\omega_\pm - \omega_\mathrm{x})}\right|} \tag{16a}$$

$$k_{\mathcal{D}\to\pm} = \frac{1}{N\hbar}(1 \pm \cos 2\phi) \frac{J(|\omega_\mathrm{x} - \omega_\pm|)}{\left|1 - e^{-\beta\hbar(\omega_\mathrm{x} - \omega_\pm)}\right|} \tag{16b}$$

$$k_{\pm\to\mp} = \frac{1}{2N\hbar} \ \sin^2 2\phi \ \frac{J(|\omega_\pm - \omega_\mp|)}{\left|1 - e^{-\beta\hbar(\omega_\pm - \omega_\mp)}\right|}. \tag{16c}$$

The above expression can also be obtained from frequency domain perturbation theory, with details provided in Ref. 72. Note that there is a large $N - 1$ fold

of degeneracy for the dark states manifold, which explicitly shows up in $k_{\pm\to\mathcal{D}}$. This may also be interpreted from the entropy perspective,[89] because Eq. 16a can be recasted as

$$k_{-\to \mathrm{D}} \approx \frac{1}{\hbar N}\cdot[1-\cos(2\Theta)]\cdot J(\omega_0-\omega_-) \times \exp\left(-\beta\left[\hbar(\omega_0-\omega_-)-k_{\mathrm{B}}T\ln(N-1)\right]\right), \tag{17}$$

such that one can define an effective entropy change $\Delta S = k_{\mathrm{B}}\ln(N-1)$ associated with the transition. Note that it differs from the thermodynamics entropy since $N-1$ is not the actual particle number but the degeneracy fold of the dark states manifold. When the dark states dominate the equilibrium population, it can be explained[89] as the dark states manifold has a relatively lower free energy than the LP, with $\Delta\mathcal{F} = \hbar(\omega_0-\omega_-) - k_{\mathrm{B}}T\ln(N-1) \equiv \Delta E - T\Delta S < 0$.

Our previous work[72] suggests that the NEFGR theory provides a reasonable estimation for all processes, although it may underestimate the rate from LP to the dark states manifold. Here, we use both rate expressions to simulate the population dynamics and the lifetime of polaritons.

B. Incorporating Cavity Loss and Excitonic Loss through Lindbladian

The HTC Hamiltonian captures the dissipation process (homogeneous broadening or dynamical disorder) via system-bath coupling (exciton-phonon interaction), as well as the important polariton relaxation process to the dark states. However, cavity loss and other relaxation channels are not included in the HTC model. Following the established methodology for Liouvillian dynamics, loss is accounted for via the addition of a Linbladian term,[45,90]

$$\frac{\mathrm{d}}{\mathrm{d}t}\hat{\rho}(t) = -\frac{i}{\hbar}[\hat{H},\hat{\rho}(t)] + \sum_\alpha \Gamma_\alpha \hat{L}_\alpha\hat{\rho}(t)\hat{L}_\alpha^\dagger - \frac{1}{2}\sum_\alpha \Gamma_\alpha\{\hat{L}_\alpha^\dagger\hat{L}_\alpha,\hat{\rho}(t)\}, \tag{18}$$

where $\hat{L}_\alpha^\dagger$ is the Lindblad jump operator associated with the decay channel α, with the corresponding rate Γ_α. As stated above, the dynamics due to the HTC Liouvillian $-\frac{i}{\hbar}[\hat{H},\hat{\rho}]$ is modeled by the FGR equation of motion, Eq. 11 (we have checked the validity of using the rate equation to model the full quantum master equation in our previous work in Ref. 72). The Lindblad jump operators $\hat{L}$ represent different relaxation channels. Since we only concern with the population dynamics of the excited states ($P_\pm$ and $P_\mathcal{D}$), the refill term $\hat{L}\hat{\rho}\hat{L}^\dagger$ can be omitted and the anti-commutator is replaced by $\{\hat{L}^\dagger\hat{L},\hat{\rho}\} = 2\hat{L}^\dagger\hat{L}\hat{\rho}$. This leaves

$$\Gamma_\alpha\hat{L}_\alpha\hat{\rho}(t)\hat{L}_\alpha^\dagger - \frac{1}{2}\Gamma_\alpha\{\hat{L}_\zeta^\dagger\hat{L}_\alpha,\hat{\rho}(t)\} \to -\Gamma_\alpha\hat{Q}_\alpha\hat{\rho}(t) \tag{19}$$

where $\hat{Q}_\alpha = \hat{L}_\alpha^\dagger\hat{L}_\alpha$.

In this study, we follow the previous work[58] that investigates polariton spectra broadening through the Lindbladian description, by considering three relaxation channels. Photonic cavity loss corresponds to

$$\hat{Q}_\mathrm{c} = |\mathrm{G},1\rangle\langle\mathrm{G},1|, \tag{20}$$

where the corresponding loss rate can be obtained from the cavity quality factor

$$\Gamma_\mathrm{c} = \omega_\mathrm{c}/\mathcal{Q}, \tag{21}$$

with $\mathcal{Q}$ as the quality factor. We also consider a local relaxation channel for each exciton site,

$$\hat{Q}_\mathrm{loc} = \sum_n |n\rangle\langle n|, \tag{22}$$

as well as a collective relaxation channel,[58]

$$\hat{Q}_\mathrm{col} = \sum_{m,n}|m\rangle\langle n| = N|B\rangle\langle B|, \tag{23}$$

with the corresponding loss rates Γ_loc and Γ_col. Detailed discussions of these Lindblad operators are provided in Appendix A.

C. Analysis of Steady State Lifetime

Casting the above $\hat{Q}$ into the polariton eigenbasis $\{|\pm\rangle, |j=1,2,\cdots N-1\rangle\}$ and keeping only the diagonal component leads to the corresponding population DOF, we have the rate equations

$$\frac{\mathrm{d}}{\mathrm{d}t}P_\pm(t) = \sum_{J\in\{\mp,\mathcal{D}\}} k_{J\to\pm}P_J(t) - k_{\pm\to J}P_\pm(t) - \Gamma_\pm P_\pm(t) \tag{24a}$$

$$\frac{\mathrm{d}}{\mathrm{d}t}P_\mathcal{D}(t) = \sum_{J\in\{\pm\}} k_{J\to\mathcal{D}}P_J(t) - k_{\mathcal{D}\to J}P_\mathcal{D}(t) - \Gamma_\mathcal{D}P_\mathcal{D}(t) \tag{24b}$$

where the loss rates $\Gamma_\pm$ are

$$\Gamma_\pm = \frac{\Gamma_\mathcal{D}}{2}(1\pm\cos 2\phi) + \frac{N\Gamma_\mathrm{col}}{2}(1\pm\cos 2\phi) + \frac{\Gamma_\mathrm{c}}{2}(1\mp\cos 2\phi) \tag{25}$$

where for the no-disorder case, $\Gamma_\mathcal{D} = \Gamma_\mathrm{loc}$. It is important to note that the $N\Gamma$ form of the collective loss component in Eq. 25 means that it corresponds to the super-radiant loss of polaritons.[56,91,92]

The relative strengths of population exchange rates $k_{I\to F}$ as well as loss rates Γ_ζ become relevant in the steady-state (SS) behavior. In the timescale of which the system reaches to the SS behavior, the population

dynamics are assumed to become fully Markovian, such that $k_{I\to F}(t) \to k_{I\to F}$. Further, the upper polariton state's population is expected to fully decay to the dark states and is supposed not to be re-populated (as transfer processes towards UP are unfavorable energetically and collectively), and lower polariton and dark state populations would have reached an unvarying, SS ratio. This hypothesis is verified by our numerical solution of the full rate equations in Eq. 24, as shown in Fig. 3 in the result section. Based on the above discussions, we have

$$\frac{\mathrm{d}}{\mathrm{d}t}\frac{P_-^{\mathrm{SS}}(t)}{P_{\mathcal{D}}^{\mathrm{SS}}(t)} = 0, \qquad \frac{P_-^{\mathrm{SS}}(t)}{P_{\mathcal{D}}^{\mathrm{SS}}(t)} \to \left(\frac{P_-}{P_{\mathcal{D}}}\right)_{\mathrm{SS}}. \tag{26}$$

Since the ratio $(P_-/P_{\mathcal{D}})_{\mathrm{SS}}$ is fixed, both populations would have the same observed loss rate Γ_{SS},

$$\frac{\mathrm{d}P_-^{\mathrm{SS}}}{\mathrm{d}t} \equiv -\Gamma_{\mathrm{SS}} P_-^{\mathrm{SS}}, \qquad \frac{\mathrm{d}P_{\mathcal{D}}^{\mathrm{SS}}}{\mathrm{d}t} \equiv -\Gamma_{\mathrm{SS}} P_{\mathcal{D}}^{\mathrm{SS}}, \tag{27}$$

where the SS behavior is defined by both $|-\rangle$ and $\mathcal{D}\rangle$ loosing population with the same rates Γ_{ss}. The actual population EOM, on the other hand, is still governed by Eq. 25. By deriving the EOM of the population sum $P_- + P_{\mathcal{D}}$ from Eq. 25, we obtain (see details in Appendix B) the expression of Γ_{SS} as

$$\Gamma_{\mathrm{SS}} = \frac{\left(\frac{P_-}{P_{\mathcal{D}}}\right)_{\mathrm{SS}}\Gamma_- + \Gamma_{\mathcal{D}}}{1 + \left(\frac{P_-}{P_{\mathcal{D}}}\right)_{\mathrm{SS}}}, \tag{28}$$

and the steady-state ratio $(P_-/P_{\mathcal{D}})_{\mathrm{SS}}$ can be obtained by solving Eq. 26 via explicitly expressing

$$\frac{\mathrm{d}}{\mathrm{d}t}\frac{P_-^{\mathrm{SS}}(t)}{P_{\mathcal{D}}^{\mathrm{SS}}(t)} = \frac{\dot{P}_-^{\mathrm{SS}}(t)P_{\mathcal{D}}^{\mathrm{SS}}(t) - P_-^{\mathrm{SS}}(t)\dot{P}_{\mathcal{D}}^{\mathrm{SS}}(t)}{[P_{\mathcal{D}}^{\mathrm{SS}}(t)]^2} = 0,$$

and substituting in the time derivatives of each population from the EOM in Eq. 24. This results in the following expression for SS population ratio

$$\left(\frac{P_-}{P_{\mathcal{D}}}\right)_{\mathrm{SS}} = \sqrt{\left(\frac{k_{\mathcal{D}\to-} + \Gamma_{\mathcal{D}} - \Gamma_-}{2k_{-\to\mathcal{D}}} - \frac{1}{2}\right)^2 + \frac{k_{\mathcal{D}\to-}}{k_{-\to\mathcal{D}}}} + \frac{k_{\mathcal{D}\to-} + \Gamma_{\mathcal{D}} - \Gamma_-}{2k_{-\to\mathcal{D}}} - \frac{1}{2}. \tag{29}$$

As such, plugging in the detailed expression of $(P_-/P_{\mathcal{D}})_{\mathrm{SS}}$ in Eq. 29 into the Γ_{SS} (Eq. 28) gives the closed form of Γ_{SS}. Eq. 29 and Eq. 28 are the *first key* results of this work.

The above SS ratio can be further simplified by working in the appropriate parameter regimes relevant to the experiments. In this study, we assume that the collective factor $N-1$ vastly overpowers the thermal energetic factor[89] $\exp[\beta(\omega_{\mathrm{x}} - \omega_-)]$, and the loss is dominated by the cavity loss process, and therefore $\Gamma_- > \Gamma_{\mathcal{D}}$. As a result, the steady-state ratio becomes

$$\left(\frac{P_-}{P_{\mathcal{D}}}\right)_{\mathrm{SS}} \approx \frac{k_{\mathcal{D}\to-}}{k_{-\to\mathcal{D}} + \Gamma_- - \Gamma_{\mathcal{D}} - k_{\mathcal{D}\to-}} < \frac{e^{\beta(\omega_{\mathrm{x}}-\omega_-)}}{N-1} \ll 1, \tag{30}$$

and the derivation of this approximate expression, as well as the SS ratio under other parameter regimes, are provided in Appendix B. This leads to the approximate steady-state loss rate

$$\Gamma_{\mathrm{SS}} \approx \Gamma_{\mathcal{D}} + k_{\mathcal{D}\to-} \Big/ \left(1 + \frac{k_{-\to\mathcal{D}}}{\Gamma_- - \Gamma_{\mathcal{D}}}\right). \tag{31}$$

Eq. 31 is the *second main result* of this work. In the collective limit where $k_{\mathcal{D}\to-} \ll \Gamma_{\mathcal{D}}$, Eq. 31 predicts that the the observed loss rate should equal to the dark-state loss rate $\Gamma_{\mathrm{SS}} \approx \Gamma_{\mathcal{D}}$, which agrees with the intuitive picture in which the dark-state manifold serves as a reservoir for the polaritons,[52] as suggested by the previous experimental work.[50,52] This also means that the *apparent* lifetime of LP, typically measured by Photoluminescence spectra, is not really determined by τ_-^{-1} (see Eq. 1), as suggested in previous literature.[52] Further, Eq. 29 and Eq. 31 are valid as long as the population dynamics are governed by a rate process, regardless of the validity of the FGR expressions for describing the rates. In this sense, we expected that Eq. 29 and Eq. 31 can be widely used to interpret the experimental data, when the rate constants and relaxation rates are extracted from kinetics equations.[49]

Note that Eq. 31 also suggests the following bound of Γ_{SS}

$$\Gamma_{\mathrm{SS}} \in \left(\Gamma_{\mathcal{D}},\ \Gamma_{\mathcal{D}} + k_{\mathcal{D}\to-}\right). \tag{32}$$

As such, for any polaritonic system (when considering a single cavity mode approximation and no-disorders), if there is a light-matter detuning dependence on the apparent lifetime $\Gamma_{\mathrm{SS}}^{-1}$ (such as those observed in Ref. 45), the current theory suggests that it is caused by $k_{\mathcal{D}\to-}$, which has to be comprable to $\Gamma_{\mathcal{D}}$ and being sensitive to the light-matter detuning.

It is also important to know the timescale at which the population dynamics is approaching the steady state for the SS analysis to be relevant. We can estimate this timescale by evaluating the rate at which $P_-/P_{\mathcal{D}}$ approaches its SS value,

$$\frac{\mathrm{d}}{\mathrm{d}t}\left[\frac{P_-(t)}{P_{\mathcal{D}}(t)} - \left(\frac{P_-}{P_{\mathcal{D}}}\right)_{\mathrm{SS}}\right] = -\tau_{\mathrm{SS}}^{-1}\left[\frac{P_-(t)}{P_{\mathcal{D}}(t)} - \left(\frac{P_-}{P_{\mathcal{D}}}\right)_{\mathrm{SS}}\right]. \tag{33}$$

Under the same collective coupling limit and cavity loss-dominated parameter regime as discussed above, the timescale approaching SS can be estimated to be

$$\tau_{\mathrm{SS}}^{-1} \approx k_{-\to\mathcal{D}} + \Gamma_- - \Gamma_{\mathcal{D}} - k_{\mathcal{D}\to-}, \tag{34}$$

which is approximately on the timescale at which lower polariton exchanges population with the dark state $k_{-\to\mathcal{D}}$. Eq. 34 is the *third* key result in this work. Again, we emphasize that the above time scale is not related to the apparent lifetime but rather how quickly the polariton system approaches the SS.

D. The effect of Disorders on Polariton Relaxation Rates

In molecular polaritons, there are various types of static disorders that exist, which will influence the polariton spectra, photophysical properties, and lienshape.[59]

We first focus our attention on dipole orientational disorder with respect to the cavity polarization direction. This results in a varied coupling strength between the photonic excitation and the matter excitation (site state) as follows

$$\langle \mathrm{G},1|\,\hat{H}\,|n\rangle = \hbar g_{\mathrm{c}}\cdot\cos\theta_n \tag{35}$$

where θ_n is the angle between the dipole vector of molecule n with respect to the cavity field polarization direction, and g_{c} is the coupling strength when the transition dipole vector is fully aligned with the field. In the present study, we consider the case of isotropic angular disorder in 3D space, in which case $\cos\theta_n$ is uniformly distributed between ±1, according to Archimedes's hatbox theorem.

Since the field-matter coupling is treated non-perturbatively in this study, it is necessary to work in the eigenbasis of the system Hamiltonian

$$\begin{aligned}\hat{H}_{\mathrm{s}}(\{\theta_n\}) &\equiv \hat{H}(\{\theta_n\}) - \hat{H}_{\mathrm{b}} - \hat{H}_{\mathrm{sb}} \\ &= \hbar\omega_{\mathrm{x}}\sum_{n=0}^{N-1}|n\rangle\langle n| + \hbar\omega_{\mathrm{c}}\,|\mathrm{G},1\rangle\langle \mathrm{G},1| \\ &\quad +\hbar g_{\mathrm{c}}\sum_{n=0}^{N-1}\cos\theta_n\Big(\,|\mathrm{G},1\rangle\langle n| + |n\rangle\langle \mathrm{G},1|\,\Big).\end{aligned} \tag{36}$$

to account for the angular disorder. Its eigenequation is

$$\hat{H}_{\mathrm{s}}(\{\theta_n\})|\tilde{\xi}\rangle = E_\xi|\tilde{\xi}\rangle. \tag{37}$$

The total Hamiltonian for the system with the dipole angular disorder is expressed as

$$\hat{H}(\{\theta_n\}) = \hat{H}_{\mathrm{s}}(\{\theta_n\}) + \hat{H}_{\mathrm{b}} + \hat{H}_{\mathrm{sb}}. \tag{38}$$

It is easy to show that the eigenstates of $\hat{H}_{\mathrm{s}}$ in Eq. 36 consist of $N-1$ degenerate dark states $|\widetilde{D}_\xi\rangle$ for $\xi\in\{1,2,\cdots N-1\}$ which are mutually orthogonal to each other, and two polariton states,[64] expressed as follows

$$|\widetilde{+}\rangle = \sin\widetilde{\phi}\;|\mathrm{G},1\rangle + \cos\widetilde{\phi}\;|\widetilde{B}\rangle \tag{39a}$$

$$|\widetilde{-}\rangle = \cos\widetilde{\phi}\;|\mathrm{G},1\rangle - \sin\widetilde{\phi}\;|\widetilde{B}\rangle\,, \tag{39b}$$

where the collective bright excitation state is

$$|\widetilde{B}\rangle = \Big(\sum_m\cos^2\theta_m\Big)^{-1/2}\cdot\sum_n\cos\theta_n\,|n\rangle\,, \tag{40}$$

and the mixing angle $\widetilde{\phi}$ is,

$$\widetilde{\phi} = \frac{1}{2}\tan^{-1}\left[\frac{2g_{\mathrm{c}}}{\omega_{\mathrm{x}}-\omega_{\mathrm{c}}}\Big(\sum_n\cos^2\theta_n\Big)^{1/2}\right]. \tag{41}$$

Henceforth, the eigenstates of $\hat{H}_{\mathrm{s}}(\{\theta_n\})$ in Eq. 36 are indexed with Greek letters $(\zeta,\xi,\cdots)$, including the polariton states in Eq. 39 as well as dark states, and the states generated with orientation disorders are marked with a tilde. The magnitude of the collective light-matter coupling is reduced compared to the disorderless case,

$$\langle\widetilde{B}|\,\hat{H}\,|\mathrm{G},1\rangle = \Big(\sum_n\cos^2\theta_n\Big)^{1/2}g_{\mathrm{c}} \le \sqrt{N}g_{\mathrm{c}}, \tag{42}$$

where for the fully ordered case, $(\sum_m\cos^2\theta_m)^{1/2}=\sqrt{N}$ and for a 3D fully isotropic case, $(\sum_m\cos^2\theta_m)^{1/2}=\sqrt{N/3}$. The reduced coupling strength leads to the corresponding reduced Rabi splitting $\widetilde{\Omega}_{\mathrm{R}}=\widetilde{\omega}_+-\widetilde{\omega}_-$, where the eigenenergies of UP and LP are

$$\widetilde{\omega}_\pm = \frac{\omega_{\mathrm{x}}+\omega_{\mathrm{c}}}{2}\pm\frac{1}{2}\sqrt{4(\sum_n\cos^2\theta_n)\cdot g_{\mathrm{c}}^2+(\omega_{\mathrm{x}}-\omega_{\mathrm{c}})^2}. \tag{43}$$

To derive the FGR rates under these angular disorders, we use the same derivation procedure reported in Ref. 72 by using $\{|\widetilde{\pm}\rangle\,,|\widetilde{\xi}\rangle\}$ as the initial and final states for rates. The phonon bath DOF, on the other hand, would still be convieneitnly expressed in the original reciprocal space for the disorderless case (c.f. Eq. 5-6), generating a set of delocalized reciprocal-space bath modes $\hat{\nu}^\dagger_{a,j}$. The asymmetrical $(j=1,2,\cdots N-1)$ bath modes are defined as

$$\hat{\nu}^\dagger_{a,j} = \frac{1}{\sqrt{N}}\sum_{n=0}^{N-1}\exp\Big(-2\pi i\,\frac{nj}{N}\Big)\hat{b}^\dagger_{a,n}, \tag{44a}$$

$$\hat{\nu}_{a,j} = \frac{1}{\sqrt{N}}\sum_{n=0}^{N-1}\exp\Big(2\pi i\,\frac{nj}{N}\Big)\hat{b}_{a,n}, \tag{44b}$$

and specifically, the symmetrical $(j=0)$ phonon bath modes are expressed as

$$\hat{\nu}^\dagger_{a,0} = \frac{1}{\sqrt{N}}\sum_{n=0}^{N-1}\hat{b}^\dagger_{a,n}. \tag{44c}$$

This leads to modifications of how both diagonal and off-diagonal system-phonon coupling could influence the transfer rates. For a disorderless system, we have shown that only the zeroth phonon mode ($\hat{\nu}^\dagger_{a,0}$, Eq. 44c) will diagonally couple to the eigenstates (see Eq. A1 in Ref. 72). In the current eigenbasis with disorders, all phonon modes in Eq. 44 will diagonally couple to the eigenbasis. In appendix D, we further show that the phonon diagonal coupling will not exceed that of the zeroth phonon in the reciprocal basis, and they will at most scale with $1/\sqrt{N}$. Hence, the effect of phonon shifts (diagonal coupling) can be ignored in the collective limit.

With the effect of diagonal system-phonon coupling ignored, the collective limit FGR rate constants in the presence of orientational disorder depend solely on the off-diagonal system-phonon coupling, in a manner similar

to the case without disorder, allowing direct comparison between the two. In the collective limit, it can be shown in Appendix C that the rate constants are *independent* of the explicit choice of dark states $\{\widetilde{D}_\xi\}$, and the expressions are related to the disorderless case (c.f. Eq. 13b) through a constant factor as follows

$$\widetilde{C}_{\pm\leftrightarrow\mathcal{D}} = \frac{N-\Delta\widetilde{N}}{N-1} C_{\pm\leftrightarrow\mathcal{D}} \quad \widetilde{C}_{\mp\to\pm} = \Delta\widetilde{N} C_{\mp\to\pm}, \quad (45)$$

where $\Delta\widetilde{N}$ depends only on the properties of the bright state as follows

$$\begin{aligned}\Delta\widetilde{N} &= \sum_{k=0}^{N-1}\left|\sum_{j=0}^{N-1}\langle j|\widetilde{B}\rangle\ \langle\widetilde{B}|j+k\rangle\right|^2 \\ &= N\frac{\sum_{n=0}^{N-1}\cos^4\theta_n}{\left(\sum_{n=0}^{N-1}\cos^2\theta_n\right)^2} > 1.\end{aligned} \quad (46)$$

Again, the tilde indicates state vectors and quantities associated with the dipole orientational disorder case, and $|D_j\rangle$ is the reciprocal basis defined in Eq. 5 (which happen to be the dark states of the no-diaordered case). Hence, the polaritonic dynamics in the presence of orientational disorder depend on the reduced field-matter coupling (Eq. 42) and the parameter $\Delta\widetilde{N}$ (Eq. 46), which in turn depends on the specific realizations of the random angles $\{\theta_n\}$.

The resulting FGR rates in the presence of angular disorder become

$$k_{\pm\to\mathcal{D}} = \frac{N-\Delta\widetilde{N}}{N\hbar}(1\pm\cos 2\widetilde{\phi})\frac{J(|\widetilde{\omega}_\pm-\omega_{\rm x}|)}{\left|1-e^{-\beta\hbar(\widetilde{\omega}_\pm-\omega_{\rm x})}\right|} \quad (47a)$$

$$k_{\mathcal{D}\to\pm} = \frac{N-\Delta\widetilde{N}}{N(N-1)\hbar}(1\pm\cos 2\widetilde{\phi})\frac{J(|\omega_{\rm x}-\widetilde{\omega}_\pm|)}{\left|1-e^{-\beta\hbar(\omega_{\rm x}-\widetilde{\omega}_\pm)}\right|} \quad (47b)$$

$$k_{\pm\to\mp} = \frac{\Delta\widetilde{N}}{2N\hbar}\ \sin^2 2\widetilde{\phi}\ \frac{J(|\widetilde{\omega}_\pm-\widetilde{\omega}_\mp|)}{\left|1-e^{-\beta\hbar(\widetilde{\omega}_\pm-\widetilde{\omega}_\mp)}\right|}, \quad (47c)$$

where $\widetilde{\omega}_\pm$ is expressed in Eq. 43. Eq. 16 is the *third* key result in this work, which suggests that the role of anular disorder for polariton relaxation is to modify $\omega_\pm-\omega_x$, $\Delta\widetilde{N}$, and the mixing angle $\widetilde{\phi}$.

As shown in Fig. 1, for a fully isotropic disordered case in 3D, the distributions of the two parameters become narrower as the number of sites N increases. Therefore, in the collective limit $N\geq 10^6$, we assume that these parameters take their expected values by replacing the sum over n in Eqs. 42, 46 with the respective integrations,

$$\frac{\langle\widetilde{B}|\,\hat{H}\,|\mathrm{G},1\rangle}{\sqrt{N}g_{\rm c}} \approx \left(\frac{1}{2}\int_{-1}^{1}\mathrm{d}\cos\theta\ \cos^2\theta\right)^{1/2} = \sqrt{\frac{1}{3}} \quad (48)$$

$$\Delta\widetilde{N} \approx \frac{2\int_{-1}^{1}\mathrm{d}\cos\theta\ \cos^4\theta}{\left(\int_{-1}^{1}\mathrm{d}\cos\theta\ \cos^2\theta\right)^2} = \frac{9}{5}, \quad (49)$$

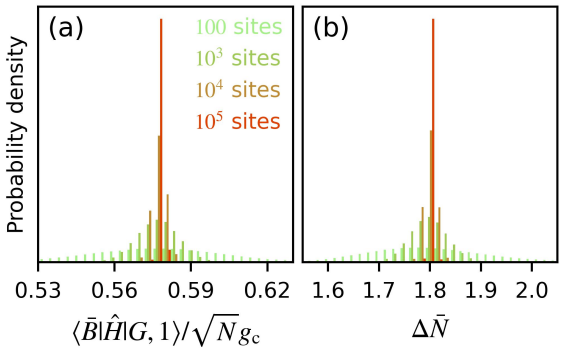

Figure 1. Distribution histograms of (a) field-matter coupling reduction ratio $\frac{\langle\widetilde{B}|\,\hat{H}\,|\mathrm{G},1\rangle}{\sqrt{N}g_{\rm c}}$, and (b) $\Delta\widetilde{N}$ as defined in Eq. 46, among different realizations (samples) of disordered site orientations $\{\theta_m\}$ with various N. The number of samples is chosen such that $N_{\rm s}\cdot N = 10^8$, with $\theta_n\in[0,2\pi]$ uniformally samled. The expected values (mean) for the plotted distributions are (a) $\left\langle\langle\widetilde{B}|\,\hat{H}\,|\mathrm{G},1\rangle\right\rangle_{\rm s}/\sqrt{N}g_{\rm c} = \sqrt{\frac{1}{3}}\approx 0.577$, and (b). $\langle\Delta\widetilde{N}\rangle = 9/5 = 1.8$.

which eliminates the need for sampling $\{\theta_n\}$. For a smaller N or some detailed realization of $\{\theta_n\}$, Eq. 43 and Eq. 46 are still needed. It is also important to note that the above angular disorder parameters reach the collective limit much more slowly than the underlying dynamics. One can infer from Fig. 1 that the distributions are not converged to the expected values at $N=100$, however, at this number of sites, the collective FGR rates Eq. 13b already become valid.

The orientational disorder does not change the effects of explicit cavity loss $\hat{Q}_{\rm cav}$ or local relaxation channel $\hat{Q}_{\rm loc}$ in the rate EOM (Eq. 24), except for the changes in the mixing angle $\phi\to\widetilde{\phi}$ and the polariton frequency $\tilde{\omega}_\pm$ (Eq. 43). To understand how the collective relaxation operator $\hat{Q}_{\rm col}$ changes with respect to the orientational disorder, we notice that since the disorder is isotropic, the new bright state $\widetilde{B}$ is expected to be orthogonal to the no-disorder bright state (Eq. 6),

$$\langle\widetilde{B}|B\rangle \propto \sum_n \cos\theta_n = 0. \quad (50)$$

Therefore, $\hat{Q}_{\rm col}$ will act solely on the dark states instead of polariton states. Following the derivation detailed in appendix A, the loss rates in the presence of angular disorder are

$$\Gamma_\pm = \frac{\Gamma_{\rm c}}{2}(1\mp\cos 2\widetilde{\phi}) + \frac{\Gamma_{\rm loc}}{2}(1\pm\cos 2\widetilde{\phi}) \quad (51a)$$

$$\Gamma_{\mathcal{D}} = \Gamma_{\rm loc} + \frac{N}{N-1}\Gamma_{\rm col}. \quad (51b)$$

As shown in the above equation, an important feature for the Lindbladian loss rates in the presence of orientational disorder is that the $\Gamma_{\rm col}$ contribution is weighted

by $N/(N-1) \to 1$ (for large N), and is thus no longer super-radiant. This is opposed to the no-disorder case in Eq. 25 where $N\Gamma_{\text{col}}$ does contribute to a super-radiant channel for $\Gamma_{\pm}$. This observation is consistent with existing theoratical[56,59,93–95] and experimental[91,96,97] studies of super-radiant polaritonic decay. Experimental observation of super-radiant polaritons is performed with well-ordered sites, either crystalline or supercooled samples in nature, and it has been demonstrated theoretically that the super-radiant loss diminishes with energetic disorder.[59] As we have shown in appendix A and Eq. 25, the super-radiant broadening arises as a natural result of simple Lindbladian radiative loss to the ground state, without the existence of inter-site coupling.[93] In a system with orientational disorder, the collective loss no longer overlaps with the bright state in the reciprocal space. It instead applies to, and has its collective-ness canceled by, the density of states of the dark-state manifold.

We would also comment on another important source of disorder in polaritonic dynamics arising from the inhomogeneous energy disorders[59,98] of exciton $\hbar\omega_x$. These static energetic disorder originates from static interactions between the exciton and the environment, which can be considered by adding the following term to the total Hamiltonian $\hat{H}$ (Eq. 2),

$$\hat{V} = \sum_{n=0}^{N-1} \epsilon_n |n\rangle\langle n|. \tag{52}$$

It has been shown that the eigenspectrum of $\hat{H}_s + \hat{V}$ can be solved exactly.[99–101] Alternatively, one often uses perturbation theory to work out the influence of $\hat{V}$. Here, we try to cast some general discussions of this type of disorder, by exactly diagonalizing the $\hat{H}_s + \hat{V}$ and obtaining its eigenstates $|\psi\rangle$, expanded in the reciprocal basis $\{|D_j\rangle\}$ (for $j = [0, N-1]$ where $|D_j\rangle \equiv |B\rangle$)

$$|\psi\rangle = \psi_\nu |\mathrm{G},1\rangle + \sum_{j=0}^{N-1} \psi_j |D_j\rangle\,;\ |\psi'\rangle = \psi'_\nu |\mathrm{G},1\rangle + \sum_{j=0}^{N-1} \psi'_j |D_j\rangle \tag{53}$$

where the expansion coefficients ψ_ν and ψ_j need to be solved numerically from diagonalizing $\hat{H} + \hat{V}$ in the $\{|\mathrm{G},1\rangle, |D_j\rangle\}$ basis. The FGR transfer rate between two such states is

$$k_{\psi\to\psi'} = \frac{2}{N\hbar} \sum_{k=0}^{N-1} \left| \sum_{j=0}^{N-1} \psi_j^* \psi'_{j+k} \right|^2 \cdot \frac{J(|\omega_\psi - \omega'_\psi|)}{|1 - e^{-\beta\hbar(\omega_\psi - \omega'_\psi)}|} \tag{54}$$

and the population dynamics can be solved numerically from the rates. This rate expression is consistent with the disorderless case. Under the limit that there is no disorder, $\psi_{j'} = \delta_{j,j'}$ is the j_{th} dark state in the reciprocal space, and $\psi'_{j'} = -\delta_{0,j'}\sin\phi$ is the disorder-less lower polariton. As a result,

$$\sum_{k=0}^{N-1} \left| \sum_{j=0}^{N-1} \psi_j^* \psi'_{j+k} \right|^2 = \frac{1}{2}(1 - \cos 2\phi)$$

which upon substitution into Eq. 54 leads to Eq. 16.

Assuming the disorder to be weak enough such that the eigenbasis comprises two polaritons and $N-1$ dark states (see the criteria discussed in Ref. 102), the inter-dark-state population transfer can be ignored during the dynamics, and the transfer rates between polaritons and dark states can be written as

$$k_{\pm\to\mathcal{D}} = \sum_{\psi'\in\mathcal{D}} k_{\pm\to\psi'}(\omega_\pm - \omega_{\psi'}) \tag{55}$$

$$k_{\mathcal{D}\to\pm} = \sum_{\psi'\in\mathcal{D}} P'_\psi k_{\psi'\to\pm}(\omega_{\psi'} - \omega_\pm) \tag{56}$$

where P'_ψ is the probability to occupy the dark state $|\psi'\rangle$, and $\sum_{\psi'} P'_\psi = 1$. For no-disorder cases, $P'_\psi = 1/(N-1)$. Further assuming that the prefactor in Eq. 54 is the same among the dark states and the relative dark state populations $P'_\psi \to P(\omega_{\psi'})$ to be a function of energy, the FGR transfer rates in this case can be approximated by a convolution,[33]

$$\langle k_{\pm\leftrightarrow\mathcal{D}}\rangle = \int \mathrm{d}\omega\ k_{\pm\leftrightarrow\mathcal{D}}(\omega)\cdot\mathcal{G}(\omega - \omega_{\mathrm{x}}), \tag{57}$$

where $\mathcal{G}(\omega - \omega_{\mathrm{x}})$ is the dark state energy distribution, and $k_{\pm\to\mathcal{D}}(\omega)$ is expressed in Eq. 54 by replacing the prefactor with a constant obtained via numerical diagonalization. One could also get an approximate analytic expression of these rates by considering these static energy disorders as perturbations. This perturbative operator will fully split the degenerated dark state manifold, and the degenerated perturbation theory is needed. Because the dark states' degeneracies are fully resolved, one, in principle, needs to compute the population dynamics between individual polaritons and dark states, instead of to a well-defined, degenerate manifold. We have developed a numerically efficient approach for this when simulating polariton spectra.[69] Here, we will not perform numerical simulations to consider the effect of static energy disorder in the following results, and only focus on the dipolar angle disorders.

III. MODEL SYSTEM AND COMPUTATIONAL DETAILS

To demonstrate the effect of various parameters on the steady-state dynamics, we study the HTC model adopted in our previous work,[72] where FGR and NE-FGR are both shown to be accurate compared to the numerically exact simulation of quantum dynamics.[72] We assume that the exciton-phonon coupling term in Eq. 3 is described by a spectral density. Each site (exciton) is coupled to a Brownian oscillator (phonon bath), with the spectral density

$$J(\omega) = \frac{4\lambda\eta\omega\Omega^2}{(\omega^2 - \Omega^2)^2 + 4\eta^2\omega^2}. \tag{58}$$

T	λ	$\hbar\Omega$	η	$\hbar\omega_x$	$\sqrt{N}\hbar g_c$
300 K	15 meV	0.2 eV	0.1 eV	2.0 eV	50 meV

Table I. Model parameters for the present study.

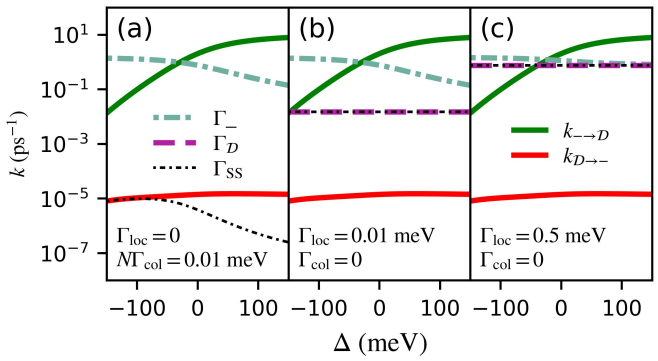

Figure 2. Semi-logarithmic plots for population exchange rates ($k_{-\leftrightarrow\mathcal{D}}$, Eq. 16), Lindbladian loss rates ($\Gamma_{-/\mathcal{D}}$), as well as steady state loss rate ($\Gamma_{\rm SS}$, Eqs. 28), against the photon-site detuning ($\Delta = \omega_c - \omega_x$). The cavity loss rate is $\Gamma_{\rm cav} = 1$ meV, which corresponds to a moderately high quality factor of $Q \approx 2000$. Three different combinations of matter losses are chosen: (a). Vanishing dark-state Lindbladian loss $\Gamma_- = 0$; (b). Finite, but slow dark-state loss; (c). Dark-state loss rate slower than, and comparable to, the cavity loss rate.

The model parameters are given in Table I, where we consider the collective limit, with $N = 10^6$, and collective light-matter coupling $\sqrt{N}g_c$.

The FGR population dynamics is obtained by solving for a simple rate equation, $(i, f, j \in \{\pm, \mathcal{D}, G\})$

$$\frac{\mathrm{d}}{\mathrm{d}t}P_j(t) = \sum_{i\neq j} k_{i\to j}P_i(t) - \sum_{f\neq j} k_{j\to f}P_j(t). \tag{59}$$

The solution of this EOM is obtained through the time-evolution matrix $\mathbf{P}(t) = \mathbf{P}(0)\exp(\mathbf{K}t)$, where K is given by

$$\mathbf{K}_{f\neq i} = k_{i\to f},\ \mathbf{K}_{Gi} = \Gamma_i,\ \mathbf{K}_{ii} = -\sum_{f\neq i}\mathbf{K}_{fi}, \tag{60}$$

where the detailed expressions for these matrix elements are provided in Eqs. 16, 51a, 51b. K is then diagonalized to become $\mathrm{K_d}$, and $\mathbf{K} = \mathbf{U}^{-1}\mathrm{K_d}\mathbf{U}$, which allows for a straightforward evaluation of population dynamics,

$$\mathbf{P}(t) = \mathbf{P}(0)\mathbf{U}^{-1}\exp(t\cdot\mathrm{K_d})\mathbf{U}. \tag{61}$$

IV. RESULTS AND DISCUSSIONS

Fig. 2 compares the transfer rates of the FGR population without disorder $k_{-\leftrightarrow\mathcal{D}}$ but include the loss rates

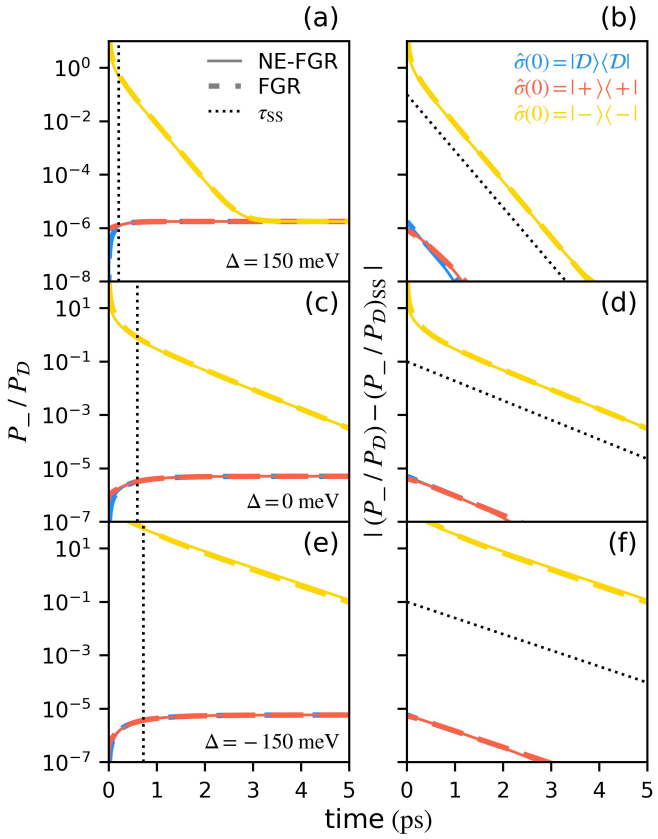

Figure 3. Semi-logarithmic plots for (a, c, e) population ratio $\frac{P_-}{P_{\mathcal{D}}}(t)$ and (b, d, f) its difference to the steady-state ratio $\left|\frac{P_-}{P_{\mathcal{D}}}(t) - \left(\frac{P_-}{P_{\mathcal{D}}}\right)_{\rm SS}\right|$. For (a, c, e), a vertical dashed line is added to the position of $\tau_{\rm SS}$. For (b, d, f), a dashed line with slope $-\tau_{\rm SS}$ is added. Lindbladian loss to chosen corresponding to Fig. 2 panel b, $\Gamma_{\rm cav} = 0.5$ meV, $\Gamma_{\rm loc} = 0.01$ meV, and $\Gamma_{\rm col} = 0$. The detuning is chosen to be $\Delta = 150$ meV for (a, b), $\Delta = 0$ for (c, d), and $\Delta = -150$ meV for (e, f).

$\Gamma_{-/\mathcal{D}}$, with the apparent loss rate in steady state $\Gamma_{\rm SS}$, and with the steady-state timescale $\tau_{\rm SS}^{-1}$. A moderately high quality factor $Q \approx 2000$ is chosen for demonstration purposes.

Fig. 2a presents the case where matter loss occurs through only the collective channel, resulting in vanishing dark-state loss rate $\Gamma_{\mathcal{D}} = 0$. According to Eq. 31, the relative magnitude of $\Gamma_{\rm SS}$ and $k_{\mathcal{D}\to-}$ depends on Γ_- and $k_{-\to\mathcal{D}}$. If $\Gamma_- \gg k_{-\to\mathcal{D}}$ (which would always be the case for realistic quality factors on the order of 10^2), $\Gamma_{\rm SS} = k_{\mathcal{D}\to-}$, which means the observed lifetime of the lower polariton would correspond to the dark-to-LP transfer rate. On the other hand, if $\Gamma_- \leq k_{-\to\mathcal{D}}$, the lower polariton lifetime would be even longer.

Fig. 2b-c presents the case where matter loss occurs only through the local channel, which corresponds to the behavior of CdSe nanoplatelets. In this case, where the dark-state Lindbladian loss is finite and much higher than $k_{\mathcal{D}\to-}$, the apparent loss $\Gamma_{\rm SS} \approx \Gamma_{\mathcal{D}}$ coincides with the

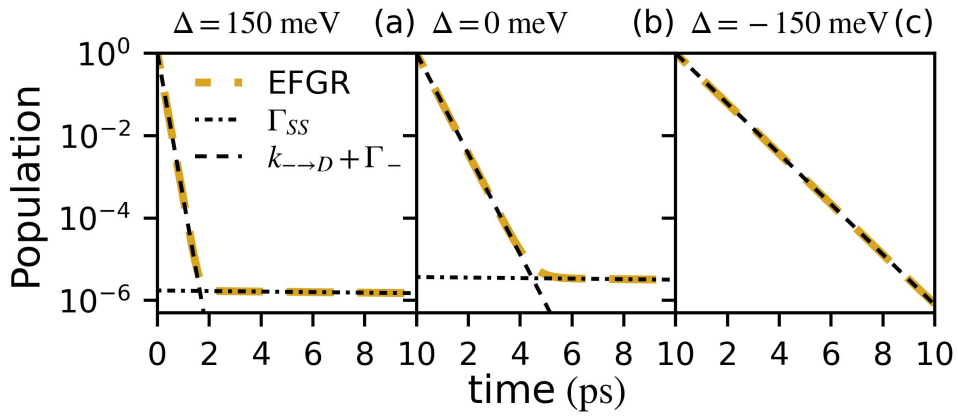

Figure 4. Log-log plots for the lower polariton population dynamics P_-, with the lower polariton being initially populated. Lindbladian loss is chosen to be the same as 3. The detuning is chosen to be (a) $\Delta = 150$ meV, (b) $\Delta = 0$, and (c) $\Delta = -150$ meV. Two black dashed lines are added to each panel with slopes of $-k_{\rm SS}$ and $-k_{-\to\mathcal{D}} - \Gamma_-$, corresponding to the steady-state loss state and the transient relaxation rate, respectively.

dark-state loss rate. This would result in a consistent steady-state lifetime that is independent of the photon energy, which can explain the apparent lack of detuning dependency on longer-timescale lifetimes in our recent experiments on CdSe nanoplatlets[45], and is consistent with experimental works where the measured polariton lifetime is close to the bare-film lifetime.[51,52] This seems to be true even if the matter loss is comparable to cavity loss (Fig. 2 c), and regardless of the relative values of Γ_- and $k_{-\to\mathcal{D}}$. In all cases demonstrated above, the observed lifetime of LP $\Gamma_{\rm SS}^{-1}$ is expected to exceed the much shorter lifetime of lossy cavities.

For the above analysis regarding the apparent lifetime to be valid, one also needs to consider the timescale $\tau_{\rm SS}$ at which the population dynamics reaches the steady state, as given in Eq. 34. Fig. 3 demonstrates the dynamics of LP-versus-dark population ratio P_- / $P_{\mathcal{D}}$, starting from either polariton $\hat{\sigma}(0) = |\pm\rangle\langle\pm|$ or dark-state manifold $\hat{\sigma}(0) = |\mathcal{D}\rangle\langle\mathcal{D}|$, which is a uniform and incoherent mixture of dark states.

Fig. 3 (b, d, f) shows the time-dependent difference between the population ratio and its steady-state value $\left|\frac{P_-}{P_{\mathcal{D}}}(t) - \left(\frac{P_-}{P_{\mathcal{D}}}\right)_{\rm SS}\right|$. This difference decays exponentially with time, with a rate of $\tau_{\rm SS}^{-1}$, meaning the steady-state timescale is an adequate description of the relaxation towards the steady state. However, the length of dynamics outside of the steady state depends heavily on the initial state. Fig. 3 (a, c, e) shows the time-dependent LP-versus-dark population ratio P_- / $P_{\mathcal{D}}$, where the time elapsed before reaching the steady state is compared directly to $\tau_{\rm SS}$. While dynamics starting from UP or the dark state reach steady state within several ($\lesssim 5$) times of $\tau_{\rm SS}$, dynamics starting from LP requires much longer time (several tens of $\tau_{\rm SS}$) to reach the SS ratio. This is because in the relevant case where the collective effect is much stronger than the thermal energetic effect, Eq. 30, the steady state ratio is much smaller than unity. If the dynamics start at LP, the initial LP-versus-dark ratio would be very large, meaning the dynamics would take longer to reach the SS. As a result, direct excitation to the lower polariton will lead to an initial period of fast relaxation that may last on the order of 10 ps, followed by (usually much slower) relaxation at $\Gamma_{\rm SS}$. In the case where the initial excitation is to a highly detuned state coupled to the exciton state, leading to an initial mixture of both polaritons, the resulting relaxation dynamics will be a more complicated mixture of fast and slow SS, leading to possibly a multi-exponential decay. This may contribute to explaining the triple-exponential relaxation observed in CdSe Nanoplatelets.[45]

Fig. 4 demonstrates the LP population dynamics of the same system, with LP being initially populated. The population graph consists of two well-defined segments of exponential decay, which show up on the log-log plots as line segments, consistent with a double-exponential relaxation dynamics. The latter half of the population follows a loss rate of $k_{\rm SS}$. This long-term relaxation rate is expected according to the steady-state analysis above (Eq. 31). The former half of the LP population follows a loss rate of $k_{-\to\mathcal{D}} + \Gamma_-$, which is the expected transient LP dynamics where population transfer from other states to LP is negligible.

As discussed in the previous section, the introduction of orientation disorder changes the population dynamics in three ways: (1). The Rabi splitting is reduced by a factor of $\sqrt{1/3}$; (2). The population exchange between polaritons and dark states slows down by a factor of $(N-1.8)/(N-1)$; (3). The collective relaxation channel no longer scales with N and affects the dark states instead of polaritons. Since we are working in the collective limit $N = 10^6$, the ratio factor $(N-1.8)/(N-1)$ can be ignored (direct population exchange between two polariton states is omitted for the same reason). The

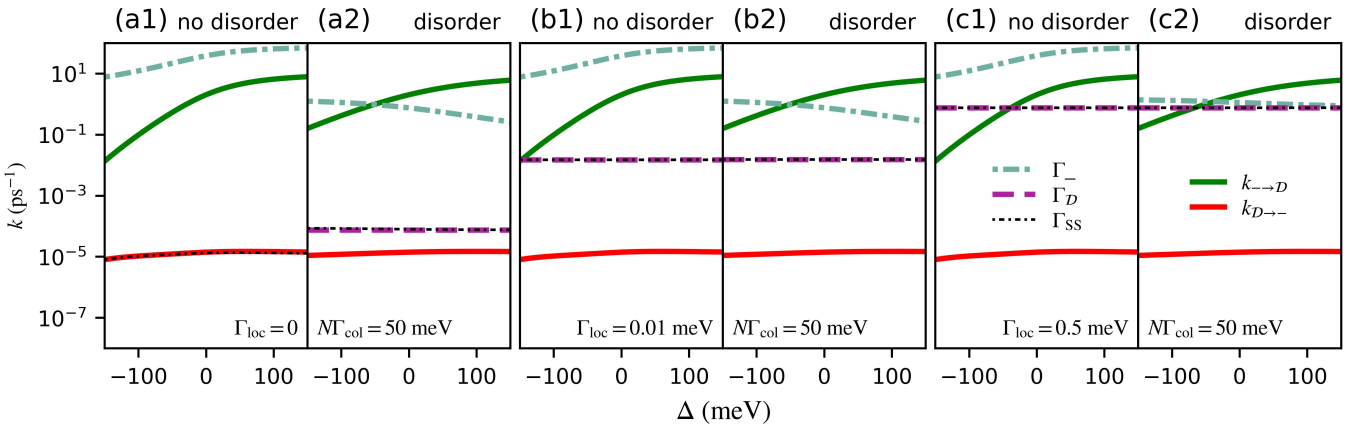

Figure 5. Semi-logarithmic plots for population exchange rates $k_{-\leftrightarrow\mathcal{D}}$, Lindbladian loss rates $\Gamma_{-/\mathcal{D}}$, as well as steady state loss rate $\Gamma_{\rm SS}$ as a function of the light-matter detuning ($\Delta = \omega_{\rm c} - \omega_{\rm x}$). The rates in the presence of isotropic orientational disorder θ_m (a2, b2, c2) are compared to the case of no disorder (a1, b1, c1). The cavity loss rate is $\Gamma_{\rm cav} = 1$ meV, which corresponds to a high quality factor of $Q \approx 2000$. The collective channel is chosen to be $N\Gamma_{\rm col} = 50$ meV, which corresponds to a bare-film radiative lifetime of $\Gamma_{\rm col}^{-1} \approx 13$ ns.

other effects of angular disorder is showcased in Fig. 5, which compares the transfer rates of the FGR population without disorder $k_{-\leftrightarrow\mathcal{D}}$ with the loss rates $\Gamma_{-/\mathcal{D}}$, the apparent loss rate in steady state $\Gamma_{\rm SS}$, and the steady-state timescale $\tau_{\rm SS}^{-1}$, with and without disorder. Compared to Fig. 2, a much faster collective loss $\Gamma_{\rm col}^{-1} \approx 13$ ps is chosen, corresponding to a realistic radiative lifetime for bare-film semiconductor nanoparticles.

The added corrections from angular disorder lead to two changes in the rates. The dependence of the FGR rates on detuning becomes weaker. This results from the weakened field-matter coupling, which decreases the dependency of $\mathcal{D}-$LP energy gap on detuning. The more important change is that of the collective loss channel. A realistic $\Gamma_{\rm col}$ value no longer leads to sub-picosecond super-radiant relaxation, and can instead be directly added to $\Gamma_{\rm loc}$ to form the apparent loss rate of LP.

V. CONCLUSION

In this work, we theoretically investigated the polariton population relaxation dynamics on a long time scale. To this end, we define the steady state (SS) of dynamics as the static LP-to-dark population ratio, and we derive a simple, analytic expressions for the SS ratio in Eq. 29, the loss rate, and the timescale within the collective limit where the collective factor $N-1$ overpowers the thermal energetic factor $\exp\beta(\omega_{\rm x} - \omega_-)$. The simple expressions in Eqs. 30, 31, 34 allow easy access to the long-term polariton lifetime from the cavity quality factor, as well as out-of-cavity spectral density and site lifetime. A more careful analysis of the steady-state reveals that the apparent SS relaxation lifetime likely coincides with the dark-state Lindbladian lifetime, which is independent of the detuning. This is consistent with several experiments that reported the prolonged lifetime of polaritons compared to the cavity loss rate. The timescale at which SS is reached depends on the initial state. Dynamics starting from UP will reach a fast SS leading to a single-exponent decay pattern, while starting from LP leads to a slow SS, where the SS dynamics come after an initial period of faster relaxation, resulting in a *double-exponent* pattern. A mixture of the two initial states would likely give more complicated relaxation patterns, which may explain the reported triple-exponent relaxation pattern for CdSe platelets.

The isotropic orientational disorder does not lead to additional computational complexities in the collective limit. The light-matter coupling and system-bath coupling parameters can both be rigorously replaced by the respective average value, eliminating the need for explicit sampling (of individual molecules' orientational disorders). The effect of orientational disorder includes a reduced Rabi splitting, as well as a non-super-radiant Lindbladian loss from the collective channel. Despite these additional theoretical changes, our analysis shows that the SS dynamics described above are still valid.

Possible future extensions of the current theory include exploring the semi-collective regime of several hundred sites, where the collective FGR rates Eq. 13b are still valid, but the orientational disorder has to be handled via explicit sampling of the site angles. Another important addition would be the case of multiple modes with different photon momenta[103–106], which makes relevant the translational symmetry or the breaking thereof. We expect this to have a complex interplay with both the translational disorder and the orientational disorder. This would be another important step towards a realistic treatment of the polaritonic relaxation dynamics.

ACKNOWLEDGMENTS

This work was supported by the Air Force Office of Scientific Research (AFOSR) under Award No. FA9550-23-1-0438, National Science Foundation Award under Grant No. CHE-2244683 and CHE-2304937, University Research Award (URA) from the University of Rochester, as well as the University of Rochester Office of the Vice President for Research, the School of Medicine and Dentistry, and Arts, Sciences & Engineering via the Center for Integrated Research Computing (CIRC). The early work of the steady-state analysis was supported by the Department of Energy under Grant No. DE-SC0022171. Computing resources were provided by the Center for Integrated Research Computing (CIRC) at the University of Rochester. We appreciate the valuable discussions with Metish Amine, Elious Mondal, and Eric Koessler on the interpretation of photoluminescence measurements and the kinetics model of steady state. We want to dedicate this work to Professor Yijing Yan, who has inspired us to explore open quantum dynamics and beyond.

CONFLICT OF INTEREST

The authors have no conflicts to disclose.

DATA AVAILABILITY

The data that support the findings of this work are available from the corresponding author upon reasonable request.

Appendix A: Lindbladian Relaxation Channels and Their Simplification under Population Only Dynamics

We start from the full Lindbladian form of loss, Eq. 18. Following convention, the relaxation operators $\hat{L}^\dagger_\alpha = \sum_a |\varnothing\rangle\langle\alpha|$ are assumed to be the hopping operators from system-relevant states $|\alpha\rangle$ to some irrelevant state $|\varnothing\rangle$ that neither directly coupled to the cavity nor transfer its population back to the system. In the present study, we consider three channels of Lindbladian relaxation,

$$\hat{L}^\dagger_{\text{cav}} = |\mathrm{G},1\rangle\langle\mathrm{G},0| \tag{A1}$$

$$\hat{L}^\dagger_{\text{loc}} = \sum_n |n\rangle\langle I_n| \tag{A2}$$

$$\hat{L}^\dagger_{\text{col}} = \sum_n |n\rangle\langle\mathrm{G},0|\,. \tag{A3}$$

Here, $\hat{L}^\dagger_{\text{cav}}$ corresponds to cavity loss where transitions occur from photonic excitation $|\mathrm{G},1\rangle$ to the ground state (vacuum) $|\mathrm{G},0\rangle$. Further, $\hat{L}^\dagger_{\text{loc}}$ corresponds to the local matter loss channel where the exciton state $|n\rangle$ hops to the corresponding irrelevant state $|I_n\rangle$, where site n occupies an irrelevant state and the other sites stay in the ground state. Examples for such irrelevant states include the double-triplet state in a singlet fission system[52] or the light-hole exciton in the CdSe nanoplatelet system.[45,75] Lastly, $\hat{L}^\dagger_{\text{loc}}$ corresponds to the local matter loss channel where the exciton state $|n\rangle$ hops to the overall ground state $|\mathrm{G},0\rangle$ directly. This is usually the radiative relaxation channel.

In the context of Lindbladian loss, we ignore the back-transition from the ground (irrelevant) state back to the system. This is equivalent to setting $\langle\mathrm{G},0|\hat{\rho}|\mathrm{G},0\rangle = \langle\mathrm{G}|\hat{\rho}|I_n\rangle = \langle I_n|\hat{\rho}|I_n\rangle = 0$ in Eq. 18. The back-flow term $\hat{L}\hat{\rho}\hat{L}^\dagger$ can be eliminated as a result, leaving

$$\frac{\mathrm{d}}{\mathrm{d}t}\hat{\rho}(t) = -\frac{i}{\hbar}[\hat{H},\hat{\rho}(t)] - \frac{1}{2}\sum_\zeta \Gamma_\zeta\{\hat{Q}_\zeta,\hat{\rho}(t)\} \tag{A4}$$

where $\hat{Q}_\zeta = \hat{L}^\dagger_\zeta\hat{L}_\zeta$. Using the expressions of $\hat{L}^\dagger$ (in Eq. A1) and explicitly working out expressions for $\hat{Q}$, we have

$$\hat{Q}_{\text{cav}} = |\mathrm{G},1\rangle\langle\mathrm{G},1| \quad \hat{Q}_{\text{loc}} = \sum_n |n\rangle\langle n| \quad \hat{Q}_{\text{col}} = \sum_{m,n} |m\rangle\langle n|\,. \tag{A5}$$

In the context of population dynamics, both $\hat{\rho}(t)$ and its derivative $\Gamma\{\hat{Q},\rho(t)\}$ are projected into the space of populations in the polaritonic basis, with

$$\Gamma\mathcal{P}\{\hat{Q},\mathcal{P}\hat{\rho}(t)\} = \Gamma\{\mathcal{P}\hat{Q},\mathcal{P}\hat{\rho}(t)\} = 2\Gamma\Big(\mathcal{P}\hat{Q}\Big)\Big(\mathcal{P}\hat{\rho}(t)\Big) \tag{A6}$$

and the anti-commutator in Eq. A6 can be replaced with the operator product since $\mathcal{P}\hat{Q}$ and $\mathcal{P}\hat{\rho}$ commute with each other.

Below, we first consider the case where there is no disorder. The projection operator is defined as

$$\mathcal{P}\hat{A} = \sum_\pm |\pm\rangle\langle\pm|\,\langle\pm|\,\hat{A}\,|\pm\rangle + \sum_j |D_j\rangle\langle D_j|\,\langle D_j|\,\hat{A}\,|D_j\rangle\,, \tag{A7}$$

with $|\pm\rangle$ expressed in Eq. 7, and $\{|D_j\rangle\}$ are expressed in Eq. 5.

Projecting all $\hat{Q}$ onto the populations and dark basis as $\mathcal{P}\hat{Q}$.

$$\begin{aligned}\mathcal{P}\hat{Q}_{\text{cav}} &= \sum_\pm |\pm\rangle\langle\pm|\,\langle\pm|\mathrm{G},1\rangle\,\langle\mathrm{G},1|\pm\rangle \\ &= \sum_\pm \frac{1}{2}\Big(1\pm\cos 2\phi\Big)\,|\pm\rangle\langle\pm|\,.\end{aligned} \tag{A8}$$

For local relaxation, no explicit resolving of the reciprocal space is required, since $\hat{Q}_{\text{loc}}$ is the identity operator in the matter subspace, and polaritons only overlap with

the bright state. One can express $\hat{Q}_{\rm loc}$ as

$$\hat{Q}_{\rm loc} = |B\rangle\langle B| + \sum_{j=1}^{N-1} |D_j\rangle\langle D_j|\,, \tag{A9}$$

where $|B\rangle$ is expressed in Eq. 6 and in the projected population subspace,

$$\mathcal{P}\hat{Q}_{\rm loc} = \sum_{\pm} \frac{1}{2}\Big(1 \mp \cos 2\phi\Big)\,|\pm\rangle\langle\pm| + \sum_{j=1}^{N-1} |D_j\rangle\langle D_j|\,. \tag{A10}$$

The collective channel $\hat{Q}_{\rm col} = \sum_{m,n} |m\rangle\langle n| = N\,|B\rangle\langle B|$ represents the super-radiant decay of the $|B\rangle$ state. In the case of no angular disorder, $|B\rangle$ is the bright state, which leads to the super-radiant decay of the polaritons,

$$\mathcal{P}\hat{Q}_{\rm col} = N\sum_{\pm} \frac{1}{2}\Big(1 \mp \cos 2\phi\Big)\,|\pm\rangle\langle\pm|\,. \tag{A11}$$

Next, we consider the case of angular disorder (Eq. 36). The projection operator is defined in the corresponding eigenbasis,

$$\widetilde{\mathcal{P}}\hat{A} = \sum_{\pm} |\widetilde{\pm}\rangle\langle\widetilde{\pm}|\,\langle\widetilde{\pm}|\,\hat{A}\,|\widetilde{\pm}\rangle + \sum_{\xi} |\widetilde{D}_\xi\rangle\langle\widetilde{D}_\xi|\,\langle\widetilde{D}_\xi|\,\hat{A}\,|\widetilde{D}_\xi\rangle \tag{A12}$$

where the polariton states $|\widetilde{\pm}\rangle$ are expressed in Eq. 39, and the dark states $\{\widetilde{D}_\xi\}$ are mutually orthogonal to each other, as well as orthogonal to $|\widetilde{\pm}\rangle$. The detailed choice of these dark states is not important in our discussion here.

For cavity loss, the projected operator $\widetilde{\mathcal{P}}\hat{Q}_{\rm cav}$ has a similiar form under isotropical orientational disorder,

$$\widetilde{\mathcal{P}}\hat{Q}_{\rm cav} = \sum_{\pm} \frac{1}{2}\Big(1 \pm \cos 2\widetilde{\phi}\Big)\,|\widetilde{\pm}\rangle\langle\widetilde{\pm}|\,. \tag{A13}$$

For local relaxation, the projected form is

$$\widetilde{\mathcal{P}}\hat{Q}_{\rm loc} = \sum_{\pm} \frac{1}{2}\Big(1 \mp \cos 2\widetilde{\phi}\Big)\,|\widetilde{\pm}\rangle\langle\widetilde{\pm}| + \sum_{\xi=1}^{N-1} |\widetilde{D}_\xi\rangle\langle\widetilde{D}_\xi|\,. \tag{A14}$$

and the structure of this operator is the same as the no-disordered case (Eq. A10).

On the other hand, with isotropical orientational disorder, the original bright state $|B\rangle$ (Eq. 6) becomes optically dark, because $\sum_n \cos\theta_n = 0$. Additionaly, we can recombine the degenerate dark states $\{|\widetilde{D}_\xi\rangle\}$ so that each dark state contains the same $j = 0$ character, meaning $|\langle\widetilde{D}_\xi|B\rangle|^2 = 1/(N-1)$ for all $\widetilde{D}_\xi$. As such, with angular disorder,

$$\widetilde{\mathcal{P}}\hat{Q}_{\rm col} = \frac{N}{N-1}\sum_{\xi=1}^{N-1} |\widetilde{D}_\xi\rangle\langle\widetilde{D}_\xi|\,, \tag{A15}$$

which is no longer super-radiant compared to the no-disorder case (Eq. A10).

Appendix B: Limits and Approximations for the Steady-State Population Ratio $(P_-/P_{\mathcal{D}})_{\rm SS}$

We provide a detailed proof of Eq. 28. In the steady state regime, the population sum $P_{\rm SS}(t) \equiv P_-(t) + P_{\mathcal{D}}(t)$ follows an exponential relaxation EOM (by using Eq. 24) as follows

$$\begin{aligned}
\frac{\mathrm{d}}{\mathrm{d}t}P_{\rm SS}(t) &= -\Gamma_- P_-(t) - \Gamma_{\mathcal{D}} P_{\mathcal{D}}(t) \qquad \text{(B1)}\\
&= -\Gamma_- \cdot \frac{(\frac{P_-}{P_{\mathcal{D}}})_{\rm SS}}{1+(\frac{P_-}{P_{\mathcal{D}}})_{\rm SS}} P_{\rm SS}(t) - \Gamma_{\mathcal{D}} \cdot \frac{1}{1+(\frac{P_-}{P_{\mathcal{D}}})_{\rm SS}} P_{\rm SS}(t)\\
&\equiv -\Gamma_{\rm SS} P_{\rm SS}(t).
\end{aligned}$$

It is straightforward to show that $P_-(t)$ and $P_{\mathcal{D}}(t)$ follow the same EOM

$$\begin{aligned}
\frac{\mathrm{d}}{\mathrm{d}t}P_-(t) &= \frac{(\frac{P_-}{P_{\mathcal{D}}})_{\rm SS}}{1+(\frac{P_-}{P_{\mathcal{D}}})_{\rm SS}} \frac{\mathrm{d}}{\mathrm{d}t}P_{\rm SS}(t) = -\Gamma_{\rm SS} P_-(t)\\
\frac{\mathrm{d}}{\mathrm{d}t}P_{\mathcal{D}}(t) &= \frac{1}{1+(\frac{P_-}{P_{\mathcal{D}}})_{\rm SS}} \frac{\mathrm{d}}{\mathrm{d}t}P_{\rm SS}(t) = -\Gamma_{\rm SS} P_{\mathcal{D}}(t)
\end{aligned} \tag{B2}$$

which are equivalent to Eq. 28. With this, we can discuss the relationship between the SS population ratio $(P_-/P_{\mathcal{D}})_{\rm SS}$ and the relative strength of $\Gamma_{\mathcal{D}}$, Γ_-, $k_{-\to\mathcal{D}}$, and $k_{\mathcal{D}\to-}$.

For the convenience of the analysis, we re-express the ratio in terms of $b = \dfrac{k_{\mathcal{D}\to-}}{k_{-\to\mathcal{D}}}$ and $a = b + \dfrac{\Gamma_{\mathcal{D}} - \Gamma_-}{k_{-\to\mathcal{D}}} - 1$, and one can easily verify that

$$\Big(\frac{P_-}{P_{\mathcal{D}}}\Big)_{\rm SS} = \frac{1}{2}\Big(\sqrt{a^2+4b} + a\Big). \tag{B3}$$

In this work, we assume that the collective effect on the rates exceeds the thermal effect,[72,89] (c.f. Eq. 17) such that

$$N \gg e^{\beta(\omega_{\rm x}-\omega_-)},$$

and as a result $b \ll 1$. We consider approximate expressions for $(P_-/P_{\mathcal{D}})_{\rm SS}$ in various limits and conditions.

Case 1. For $a < 0$ and $a^2 \gg 4b$. This is the condition adopted in the main text, where we assume that Lindbladian relaxation is dominated by cavity loss $\Gamma_{\rm c} \gg \Gamma_{\rm loc}, N\Gamma_{\rm col}$, and as a result $\Gamma_- > \Gamma_{\mathcal{D}}$.

$$\begin{aligned}
\Big(\frac{P_-}{P_{\mathcal{D}}}\Big)_{\rm SS} &= \frac{2b}{\sqrt{a^2+4b}+a} \approx -\frac{b}{a}\\
&= \frac{k_{\mathcal{D}\to-}}{k_{-\to\mathcal{D}} + \Gamma_- - \Gamma_{\mathcal{D}} - k_{\mathcal{D}\to-}}.
\end{aligned} \tag{B4}$$

Case 1a. For $(\Gamma_- - \Gamma_{\mathcal{D}}) \gg k_{-\to\mathcal{D}}$. This is a stronger condition than above, where the dynamics are dominated by Lindbladian loss,

$$\Big(\frac{P_-}{P_{\mathcal{D}}}\Big)_{\rm SS} \approx \frac{k_{\mathcal{D}\to-}}{\Gamma_- - \Gamma_{\mathcal{D}}}. \tag{B5}$$

Case 1b. For $k_{-\to\mathcal{D}} \gg (\Gamma_- - \Gamma_{\mathcal{D}}) \geq -k_{\mathcal{D}\to-}$. The inverse of the above condition, where the Lindbladian loss is negligible compared to population transfer. This results in a steady-state population ratio that coincides with detailed balance

$$\left(\frac{P_-}{P_{\mathcal{D}}}\right)_{\rm SS} \approx \frac{k_{\mathcal{D}\to-}}{k_{-\to\mathcal{D}}} = \frac{e^{\beta\hbar(\omega_{\rm x}-\omega_-)}}{N-1}. \tag{B6}$$

Case 2. For $a > 0$, and $a^2 \gg 4b$. The alternative conditions (2, 2a) are included here for completeness.

$$\begin{aligned}\left(\frac{P_-}{P_{\mathcal{D}}}\right)_{\rm SS} &= \frac{\sqrt{a^2+4b}+a}{2} \approx a \\ &= \frac{k_{\mathcal{D}\to-}+\Gamma_{\mathcal{D}}-\Gamma_- - k_{-\to\mathcal{D}}}{k_{-\to\mathcal{D}}}.\end{aligned} \tag{B7}$$

Case 2a. For $(\Gamma_{\mathcal{D}} - \Gamma_-) \gg k_{-\to\mathcal{D}}$. Then we can show that

$$\left(\frac{P_-}{P_{\mathcal{D}}}\right)_{\rm SS} \approx \frac{\Gamma_{\mathcal{D}}-\Gamma_-}{k_{-\to\mathcal{D}}}. \tag{B8}$$

Further, to evaluate $\tau_{\rm SS}^{-1}$ (c.f. Eq. 33) , which is the rate for the system to approach the steady state behavior, we start with the EOM of the population ratio between LP and dark state as follows

$$\frac{\mathrm{d}}{\mathrm{d}t}\frac{P_-(t)}{P_{\mathcal{D}}(t)} = -k_{-\to\mathcal{D}}\left(\frac{P_-(t)}{P_{\mathcal{D}}(t)}\right)^2 - \left(k_{-\to\mathcal{D}}+\Gamma_- - \Gamma_{\mathcal{D}} - k_{\mathcal{D}\to-}\right)\frac{P_-(t)}{P_{\mathcal{D}}(t)} + k_{\mathcal{D}\to-} \tag{B9}$$

also,

$$-k_{-\to\mathcal{D}}\left(\frac{P_-}{P_{\mathcal{D}}}\right)_{\rm SS}^2 - \left(k_{-\to\mathcal{D}}+\Gamma_- - \Gamma_{\mathcal{D}} - k_{\mathcal{D}\to-}\right)\left(\frac{P_-}{P_{\mathcal{D}}}\right)_{\rm SS} + k_{\mathcal{D}\to-} = 0. \tag{B10}$$

Taking the difference between the two yields

$$\begin{aligned}\frac{\mathrm{d}}{\mathrm{d}t}\left[\frac{P_-(t)}{P_{\mathcal{D}}(t)} - \left(\frac{P_-}{P_{\mathcal{D}}}\right)_{\rm SS}\right] &= -k_{-\to\mathcal{D}}\left[\frac{P_-(t)}{P_{\mathcal{D}}(t)} + \left(\frac{P_-}{P_{\mathcal{D}}}\right)_{\rm SS}\right]\left[\frac{P_-(t)}{P_{\mathcal{D}}(t)} - \left(\frac{P_-}{P_{\mathcal{D}}}\right)_{\rm SS}\right] \\ &\quad -\left(k_{-\to\mathcal{D}}+\Gamma_- - \Gamma_{\mathcal{D}} - k_{\mathcal{D}\to-}\right)\left[\frac{P_-(t)}{P_{\mathcal{D}}(t)} - \left(\frac{P_-}{P_{\mathcal{D}}}\right)_{\rm SS}\right] \\ &\equiv \tau_{\rm SS}^{-1}\left[\frac{P_-(t)}{P_{\mathcal{D}}(t)} - \left(\frac{P_-}{P_{\mathcal{D}}}\right)_{\rm SS}\right]\end{aligned} \tag{B11}$$

Assuming the state of the system is close to the steady-state $P_-(t)/P_{\mathcal{D}}(t) \to (P_-/P_{\mathcal{D}})_{\rm SS}$ and substitute in Eq. 29 yields

$$\tau_{\rm SS}^{-1} = \sqrt{(k_{-\to\mathcal{D}}+\Gamma_- - \Gamma_{\mathcal{D}} - k_{\mathcal{D}\to-})^2 + 4k_{-\to\mathcal{D}}k_{\mathcal{D}\to-}} \tag{B12}$$

which reduces to $\tau_{\rm SS}^{-1} = k_{-\to\mathcal{D}} + \Gamma_- - \Gamma_{\mathcal{D}} - k_{\mathcal{D}\to-}$ with the assumption of $k_{-\to\mathcal{D}} \gg k_{\mathcal{D}\to-}$ and $\Gamma_- > \Gamma_{\mathcal{D}}$.

Appendix C: Derivation of NE-FGR rates with Dipole Angular Disorder

The key component of the FGR rate constats $C_{i\to f}(t,s)$ is expressed as the following two-time correlation functions,

$$C_{i\to f}(t,s) = \mathrm{Tr}\left[\hat{\rho}_{\rm b}(0)e^{\frac{i}{\hbar}\hat{H}_i t}\hat{H}_{if}e^{-\frac{i}{\hbar}\hat{H}_f s}\hat{H}_{fi}e^{-\frac{i}{\hbar}\hat{H}_i(t-s)}\right] \tag{C1}$$

where $\hat{\rho}_{\rm b}(0)$ is the thermal distribution of the phonons without coupling to excitons

$$\hat{\rho}_{\rm b}(0) = \bigotimes_a \bigotimes_{j=0}^{N-1} \frac{1}{\mathcal{Z}_{a,j}}\exp\left(-\beta\hat{h}_a^j\right) \tag{C2}$$

Following our previous work in Ref. 72, we expand the Hamiltonian (Eq. 38) into single phonon-mode components

$$\hat{H}_\zeta = \langle\widetilde{\zeta}|\,\hat{H}\,|\widetilde{\zeta}\rangle = \hbar\omega_\zeta + \sum_a\sum_{j=0}^{N-1}\hat{h}_a^j + \sum_a \hat{H}_{a,\zeta} \tag{C3a}$$

$$\hat{H}_{\zeta\xi} = \langle\widetilde{\zeta}|\,\hat{H}\,|\widetilde{\xi}\rangle = \sum_a \hat{H}_{a,\zeta\xi} \tag{C3b}$$

$$\hat{h}_a^j = \hbar\omega_a\hat{\nu}_{a,j}^\dagger\hat{\nu}_{a,j} \tag{C3c}$$

where $|\widetilde{\zeta}\rangle = \{|\widetilde{\pm}\rangle, |\widetilde{D}_\zeta\rangle\}$ are eigenvectors of $\hat{H}_{\rm s}(\{\theta_n\})$ (see Eq. 37). Further, the detailed expressions of $\hat{H}_{a,\zeta}$ and

$\hat{H}_{a,\zeta\xi}$ are expressed as

$$\hat{H}_{a,\zeta} = \frac{c_a}{\sqrt{N}} \sum_{k=0}^{N-1} (\hat{\nu}_k^\dagger + \hat{\nu}_{-k}) \sum_{j=0}^{N-1} c_{\zeta,j}^* c_{\zeta,j+k} \tag{C4a}$$
$$\equiv \frac{c_a}{\sqrt{N}} \sum_{k=0}^{N-1} S_{\zeta\zeta,k} (\hat{\nu}_k^\dagger + \hat{\nu}_{-k})$$
$$\hat{H}_{a,\zeta\xi} = \frac{c_a}{\sqrt{N}} \sum_{k=0}^{N-1} (\hat{\nu}_k^\dagger + \hat{\nu}_{-k}) \sum_{j=0}^{N-1} c_{\zeta,j}^* c_{\xi,j+k} \tag{C4b}$$
$$\equiv \frac{c_a}{\sqrt{N}} \sum_{k=0}^{N-1} S_{\zeta\xi,k} (\hat{\nu}_k^\dagger + \hat{\nu}_{-k}),$$

where $c_{\zeta,j} = \langle \widetilde{\zeta} | D_j \rangle$ is the overlap between the exciton eigenstates with and without disorder, and $S_{\zeta\xi,k} \equiv c_{\zeta,j}^* c_{\xi,j+k}$.

For the brevity of the derivation, the reciprocal space index $\{j, k, \cdots\}$ is defined cyclically so that $-j \equiv N - j$ and $N + j \equiv j$. As shown in appendix D, the diagonal system-bath coupling parameter $S_{\zeta\zeta,k}$ have an upper bound of

$$S_{\zeta\zeta,k} \leq S_{\zeta\zeta,0} = 1. \tag{C5}$$

Following our previous work,[72] all diagonal system-bath coupling $\hat{H}_{a,\zeta}$ can be omitted in the limit of $N \to \infty$. This greatly simplifies the correlation function $C_{i\to f}$ into a multiplication of $C_{D\to D}(s)$. Assuming the dark states to be initially unpopulated, the relevant transfer rates are simplified to (the overbar on $\widetilde{C}$ is to signify the existence of orientational disorder),

$$\widetilde{C}_{\zeta\to\xi}(t,s) = \sum_{j=0}^{N-1} |S_{\zeta\xi,j}|^2 \sum_a \frac{c_a^2}{N} \Big(\langle \hat{\nu}_a^\dagger(s) \hat{\nu}_a \rangle + \langle \hat{\nu}_a(s) \hat{\nu}_a^\dagger \rangle \Big)$$
$$\equiv \sum_{j=0}^{N-1} |S_{\zeta\xi,j}|^2 C_{D\to D}(s) = \widetilde{C}_{\xi\to\zeta}(t,s) \tag{C6}$$

$$\widetilde{C}_{\pm\to\zeta}(t,s) = e^{i(\omega_x - \omega_\pm)s} \frac{1}{2}(1 \pm \cos 2\widetilde{\phi})$$
$$\times \sum_{j=0}^{N-1} |S_{0\zeta,j}|^2 \sum_a \frac{c_a^2}{N} \Big(\langle \hat{\nu}_a^\dagger(s) \hat{\nu}_a \rangle + \langle \hat{\nu}_a(s) \hat{\nu}_a^\dagger \rangle \Big) \tag{C7}$$
$$\equiv e^{i(\omega_x - \omega_\pm)s} \frac{1}{2}(1 \pm \cos 2\widetilde{\phi}) \sum_{j=0}^{N-1} |S_{0\zeta,j}|^2 C_{D\to D}(s)$$

Since the $N-1$ dark states are degenerate, a non-unique choice of basis has to be made for the explicit evaluation of individual transfer rates. To combine the dark-state populations into one manifold population, as in the case of no disorder, a set of dark states has to be chosen such that their population stays the same. This, since forward and backward transfer rates are always equal between any pairs of dark states, is equivalent to requiring $\sum_j |S_{0\zeta,j}|^2$ to be equal for all $\zeta \neq 0$, which makes the dark states equivalent in terms of the transfer rates between them and the polaritons. To this end, we consider the sum of these rates over all dark states and realize that it is independent of the choice of dark states

$$\sum_{\zeta=1}^{N-1} \sum_{j=0}^{N-1} |S_{0\zeta,j}|^2 = N - \sum_{k=0}^{N-1} \Big| \sum_{j=0}^{N-1} c_{0,j}^* c_{0,j+k} \Big|^2 \tag{C8}$$
$$\equiv N - \Delta\widetilde{N}$$

Since it is always possible to recombine the dark states into a new basis such that they have the same population, we assume (without explicitly specifying the basis) that such a dark-state basis is always taken, and that the transfer rates between singular dark-state and polariton are $1/(N-1)$ of their corresponding sum, which is independent of the dark-state choice,

$$\widetilde{C}_{\pm\to\mathcal{D}}(t,s) = e^{i(\omega_x - \omega_\pm)s} \frac{1}{2}(1 \pm \cos 2\widetilde{\phi})(N - \Delta\widetilde{N}) C_{D\to D}(s)$$
$$\widetilde{C}_{\mathcal{D}\to\pm}(t,s) = e^{i(\omega_\pm - \omega_x)s} \frac{1}{2}(1 \pm \cos 2\widetilde{\phi}) \frac{N - \Delta\widetilde{N}}{N-1} C_{D\to D}(s) \tag{C9}$$

which, upon Fourier transformation, leads to the polariton-dark transfer rates being under the collective limit.

The population transfer rate constant between the polaritons is given by,

$$\widetilde{C}_{\pm\to\mp}(t,s) = e^{i(\omega_\pm - \omega_\mp)s} \frac{1}{4} \sin^2 2\widetilde{\phi} \sum_{j=0}^{N-1} |S_{00,j}|^2 C_{D\to D}(s)$$
$$= e^{i(\omega_\pm - \omega_\mp)s} \frac{1}{4} \sin^2 2\widetilde{\phi}\ \Delta\widetilde{N}\ C_{D\to D}(s) \tag{C10}$$

For fully isotropic orientational disorder, the value of $\Delta\widetilde{N}$ can be obtained via integration over $\cos\theta$, without generating the bright state from explicit sampling of $\{\theta_m\}$.

Appendix D: Proof that shift of phonon modes has an upper bound in the presence of angular disorder

Here, we provide proof that the diagonal shift due to coupling to the phonon modes has an upper bound in the presence of angular disorder (Eq. C5). It is easy to see that $S_{\zeta\zeta,0} = 1$. In this section, we will show that this is an upper bound for all phonon mode shifts in the reciprocal states, under any eigenstate, i.e.,

$$S_{\zeta\zeta,0} = \sum_{j=0}^{N-1} c_{\zeta,j}^* c_{\zeta,j} \geq \Big| \sum_{j=0}^{N-1} c_{\zeta,j}^* c_{\zeta,j+k} \Big| = |S_{\zeta\zeta,k}| \tag{D1}$$

This would be achieved by proving the stronger statement that

$$\sum_{j=0}^{N-1} |c_{\zeta,j}|^2 \geq \sum_{j=0}^{N-1} |c_{\zeta,j}| |c_{\zeta,p(j)}| \tag{D2}$$

for any $\{p(0), p(1), \cdots\}$ which is a permutation of $\{0, 1, \cdots N-1\}$, such that $\{c_{\zeta,p(j)}\}$ is a permutation of $\{c_{\zeta,j}\}$.

Assuming Eq. D2 is true for $N = 1, 2, \cdots M$, we consider the case of $N = M+1$. We realize that a unique directed graph can be constructed for any permutation $\{p(0), p(1), \cdots\}$, starting from N labeled vertices $\{v_0, v_1, \cdots\}$, and construct a directed edge from every j to $p(j)$. The resulting graph is a disjoint union of one or more branchless directed cycles. In the case of more than one cycles $\mathbb{V}$, Eq. D2 can be proved by splitting the sum accordingly,

$$\begin{aligned}\sum_{j=0}^{M}|c_{\zeta,j}||c_{\zeta,p(j)}| &= \sum_{\mathbb{V}}\sum_{j\in\mathbb{V}}|c_{\zeta,j}||c_{\zeta,p(j)}| \\ \leq \sum_{\mathbb{V}}\sum_{j\in\mathbb{V}}|c_{\zeta,j}|^2 &= \sum_{j=0}^{M}|c_{\zeta,j}|^2\end{aligned} \tag{D3}$$

This leaves us with the case of one singular cycle of size $M+1$. Without loss of generality, we assign $|c_{\zeta,0}|$ to be the largest $|c|$ term by permuting them along the $M+1-$ cycle. Removing this largest term and constructing an $M-$ cycle leads to

$$\begin{aligned}&\sum_{j=0}^{M}|c_{\zeta,j}||c_{\zeta,p(j)}| \\ &\quad= |c_{\zeta,0}||c_{\zeta,p(0)}| + |c_{\zeta,p^{-1}(0)}||c_{\zeta,0}| \\ &\qquad -|c_{\zeta,p^{-1}(0)}||c_{\zeta,p(0)}| \\ &\qquad +\sum_{j,p(j)\neq 0}|c_{\zeta,j}||c_{\zeta,p(j)}| + |c_{\zeta,p^{-1}(0)}||c_{\zeta,p(0)}| \\ &\quad\leq |c_{\zeta,0}||c_{\zeta,p(0)}| + |c_{\zeta,p^{-1}(0)}||c_{\zeta,0}| \\ &\qquad -|c_{\zeta,p^{-1}(0)}||c_{\zeta,p(0)}| + \sum_{j\neq 0}|c_{\zeta,j}|^2 \\ &\quad= \Big(|c_{\zeta,0}| - |c_{\zeta,p(0)}|\Big)\Big(|c_{\zeta,p^{-1}(0)}| - |c_{\zeta,0}|\Big) \\ &\qquad +\sum_{j=0}^{M}|c_{\zeta,j}|^2 \\ &\quad\leq \sum_{j=0}^{M}|c_{\zeta,j}|^2,\end{aligned} \tag{D4}$$

which completes the proof of the induction step. Since the base case of $N = 1, 2$ is obvious, by induction we conclude that Eq. D2 holds in general. By defining the permutation to be $p(j) = j + k$, the original statement can be easily obtained:

$$\begin{aligned}S_{\zeta\zeta,0} &= \sum_{j=0}^{N-1} c^*_{\zeta,j}c_{\zeta,j} \\ &\geq \sum_{j=0}^{N-1}|c_{\zeta,j}||c_{\zeta,j+k}| = \sum_{j=0}^{N-1}|c^*_{\zeta,j}c_{\zeta,j+k}| \\ &\geq \Big|\sum_{j=0}^{N-1} c^*_{\zeta,j}c_{\zeta,j+k}\Big| = |S_{\zeta\zeta,k}|.\end{aligned} \tag{D5}$$

REFERENCES

[1] A. Mandal, M. A. Taylor, B. M. Weight, E. R. Koessler, X. Li, and P. Huo, "Theoretical advances in polariton chemistry and molecular cavity quantum electrodynamics," Chem. Rev. **123**, 9786–9879 (2023).

[2] M. A. Zeb, P. G. Kirton, and J. Keeling, "Exact states and spectra of vibrationally dressed polaritons," ACS Photonics **5**, 249–257 (2018), https://doi.org/10.1021/acsphotonics.7b00916.

[3] A. Kavokin and G. Malpuech, ***Cavity polaritons*** (Elsevier, San Diego, 2003).

[4] J. A. Hutchison, T. Schwartz, C. Genet, E. Devaux, and T. W. Ebbesen, "Modifying chemical landscapes by coupling to vacuum fields," Angew. Chem. Int. Edit. **51**, 1592–1596 (2012).

[5] H. Zeng, J. B. Pérez-Sánchez, C. T. Eckdahl, P. Liu, W. J. Chang, E. A. Weiss, J. A. Kalow, J. Yuen-Zhou, and N. P. Stern, "Control of photoswitching kinetics with strong light–matter coupling in a cavity," J. Am. Chem. Soc. **145**, 19655–19661 (2023), pMID: 37643086.

[6] I. Lee, S. R. Melton, D. Xu, and M. Delor, "Controlling molecular photoisomerization in photonic cavities through polariton funneling," J. Am. Chem. Soc. **146**, 9544–9553 (2024).

[7] A. Mandal and P. Huo, "Investigating new reactivities enabled by polariton photochemistry," J. Phys. Chem. Lett. **10**, 5519–5529 (2019), pMID: 31475529.

[8] K. Stranius, M. Hertzog, and K. Börjesson, "Selective manipulation of electronically excited states through strong light–matter interactions," Nat. Commun. **9**, 2273 (2018).

[9] A. Canaguier-Durand, C. Genet, A. Lambrecht, T. W. Ebbesen, and S. Reynaud, "Non-markovian polariton dynamics in organic strong coupling," Eur. Phys. J. D **69**, 24 (2015).

[10] E. R. Koessler, A. Mandal, A. J. Musser, T. D. Krauss, and P. Huo, "Polariton mediated electron transfer under the collective molecule-cavity coupling regime," Chem. Sci. **16**, 11644–11658 (2025).

[11] D. Xu, A. Mandal, J. M. Baxter, S.-W. Cheng, I. Lee, H. Su, S. Liu, D. R. Reichman, and M. Delor, "Ultrafast imaging of polariton propagation and interactions," Nat. Commun. **14**, 3881 (2023).

[12] R. H. Tichauer, I. Sokolovskii, and G. Groenhof, "Tuning the coherent propagation of organic exciton-polaritons through the cavity q-factor," Adv. Sci. **10** (2023), 10.1002/advs.202302650.

[13] I. Sokolovskii, R. H. Tichauer, D. Morozov, J. Feist, and G. Groenhof, "Multi-scale molecular dynamics simulations of enhanced energy transfer in organic molecules under strong coupling," Nat. Commun. **14**, 6613 (2023).

[14] R. Pandya, A. Ashoka, K. Georgiou, J. Sung, R. Jayaprakash, S. Renken, L. Gai, Z. Shen, A. Rao, and A. J. Musser, "Tuning the coherent propagation of organic exciton-polaritons through dark state delocalization," Adv. Sci. **9** (2022), 10.1002/advs.202105569.

[15] R. Pandya, R. Y. S. Chen, Q. Gu, J. Sung, C. Schnedermann, O. S. Ojambati, R. Chikkaraddy, J. Gorman, G. Jacucci, O. D. Onelli, T. Willhammar, D. N. Johnstone, S. M. Collins, P. A. Midgley, F. Auras, T. Baikie, R. Jayaprakash, F. Mathevet,

R. Soucek, M. Du, A. M. Alvertis, A. Ashoka, S. Vignolini, D. G. Lidzey, J. J. Baumberg, R. H. Friend, T. Barisien, L. Legrand, A. W. Chin, J. Yuen-Zhou, S. K. Saikin, P. Kukura, A. J. Musser, and A. Rao, "Microcavity-like exciton-polaritons can be the primary photoexcitation in bare organic semiconductors," Nat. Commun. **12**, 6519 (2021).

[16]Y. Zakharko, M. Rother, A. Graf, B. Hähnlein, M. Brohmann, J. Pezoldt, and J. Zaumseil, "Radiative pumping and propagation of plexcitons in diffractive plasmonic crystals," Nano Lett. **18**, 4927–4933 (2018).

[17]G. G. Rozenman, K. Akulov, A. Golombek, and T. Schwartz, "Long-range transport of organic exciton-polaritons revealed by ultrafast microscopy," ACS Photonics **5**, 105–110 (2018).

[18]G. Lerario, A. Fieramosca, F. Barachati, D. Ballarini, K. S. Daskalakis, L. Dominici, M. D. Giorgi, S. A. Maier, G. Gigli, S. Kéna-Cohen, and D. Sanvitto, "Room-temperature superfluidity in a polariton condensate," Nat. Phys. **13**, 837–841 (2017).

[19]A. Gianfrate, L. Dominici, O. Voronych, M. Matuszewski, M. Stobińska, D. Ballarini, M. D. Giorgi, G. Gigli, and D. Sanvitto, "Superluminal x-waves in a polariton quantum fluid," Light Sci. Appl. **7**, 17119–17119 (2017).

[20]M. Sich, D. N. Krizhanovskii, M. S. Skolnick, A. V. Gorbach, R. Hartley, D. V. Skryabin, E. A. Cerda-Méndez, K. Biermann, R. Hey, and P. V. Santos, "Observation of bright polariton solitons in a semiconductor microcavity," Nat. Photonics **6**, 50–55 (2012).

[21]T. Freixanet, B. Sermage, A. Tiberj, and R. Planel, "In-plane propagation of excitonic cavity polaritons," Phys. Rev. B **61**, 7233–7236 (2000).

[22]J. D. Plumhof, T. Stöferle, L. Mai, U. Scherf, and R. F. Mahrt, "Room-temperature bose–einstein condensation of cavity exciton–polaritons in a polymer," Nat. Mater. **13**, 247–252 (2014).

[23]H. Deng, H. Haug, and Y. Yamamoto, "Exciton-polariton bose-einstein condensation," Rev. Mod. Phys. **82**, 1489–1537 (2010).

[24]J. Keeling, F. M. Marchetti, M. H. Szymańska, and P. B. Littlewood, "Collective coherence in planar semiconductor microcavities," Semicond. Sci. Tech. **22**, R1–R26 (2007).

[25]S. Ghosh and T. C. H. Liew, "Quantum computing with exciton-polariton condensates," npj Quantum Inf. **6**, 16 (2020).

[26]N. Y. Kim and Y. Yamamoto, "Exciton-polariton quantum simulators," in ***Quantum Simulations with Photons and Polaritons: Merging Quantum Optics with Condensed Matter Physics***, edited by D. G. Angelakis (Springer International Publishing, Cham, 2017) pp. 91–121.

[27]W. Ahn, J. F. Triana, F. Recabal, F. Herrera, and B. S. Simpkins, "Modification of ground-state chemical reactivity via light–matter coherence in infrared cavities," Science **380**, 1165–1168 (2023).

[28]A. Sau, K. Nagarajan, B. Patrahau, L. Lethuillier-Karl, R. M. A. Vergauwe, A. Thomas, J. Moran, C. Genet, and T. W. Ebbesen, "Modifying woodward–hoffmann stereoselectivity under vibrational strong coupling," Angew. Chem. Int. Edit. **60**, 5712–5717 (2021).

[29]K. Nagarajan, A. Thomas, and T. W. Ebbesen, "Chemistry under vibrational strong coupling," J. Am. Chem. Soc. **143**, 16877–16889 (2021).

[30]B. Munkhbat, M. Wersäll, D. G. Baranov, T. J. Antosiewicz, and T. Shegai, "Suppression of photo-oxidation of organic chromophores by strong coupling to plasmonic nanoantennas," Sci. Adv. **4**, eaas9552 (2018).

[31]R. F. Ribeiro, L. A. Martínez-Martínez, M. Du, J. Campos-Gonzalez-Angulo, and J. Yuen-Zhou, "Polariton chemistry: controlling molecular dynamics with optical cavities," Chem. Sci. **9**, 6325–6339 (2018).

[32]W. Ying and P. Huo, "Resonance theory and quantum dynamics simulations of vibrational polariton chemistry," J. Chem. Phys. **159**, 084104 (2023).

[33]W. Ying, M. A. D. Taylor, and P. Huo, "Resonance theory of vibrational polariton chemistry at the normal incidence," Nanophotonics **13**, 2601–2615 (2024).

[34]D. Hu, W. Ying, and P. Huo, "Resonance enhancement of vibrational polariton chemistry obtained from the mixed quantum-classical dynamics simulations," J. Phys. Chem. Lett. **14**, 11208–11216 (2023).

[35]W. Ying and P. Huo, "Resonance theory of vibrational strong coupling enhanced polariton chemistry and the role of photonic mode lifetime," Commun. Mater. **5**, 110 (2024).

[36]S. Montillo Vega, W. Ying, and P. Huo, "Theoretical insights into the resonant suppression effect in vibrational polariton chemistry," J. Am. Chem. Soc. **147**, 19727–19737 (2025).

[37]S. Renken, R. Pandya, K. Georgiou, R. Jayaprakash, L. Gai, Z. Shen, D. G. Lidzey, A. Rao, and A. J. Musser, "Untargeted effects in organic exciton–polariton transient spectroscopy: A cautionary tale," J. Chem. Phys. **155**, 154701 (2021), https://pubs.aip.org/aip/jcp/article-pdf/doi/10.1063/5.0063173/14729086/154701_1_online.pdf.

[38]C. A. DelPo, B. Kudisch, K. H. Park, S.-U.-Z. Khan, F. Fassioli, D. Fausti, B. P. Rand, and G. D. Scholes, "Polariton transitions in femtosecond transient absorption studies of ultrastrong light–molecule coupling," The Journal of Physical Chemistry Letters **11**, 2667–2674 (2020), pMID: 32186878, https://doi.org/10.1021/acs.jpclett.0c00247.

[39]T. Schwartz, J. A. Hutchison, J. Léonard, C. Genet, S. Haacke, and T. W. Ebbesen, "Polariton dynamics under strong light–molecule coupling," ChemPhysChem **14**, 125–131 (2013).

[40]N. Somaschi, L. Mouchliadis, D. Coles, I. E. Perakis, D. G. Lidzey, P. G. Lagoudakis, and P. G. Savvidis, "Ultrafast polariton population build-up mediated by molecular phonons in organic microcavities," Appl. Phys. Lett **99**, 143303 (2011), https://pubs.aip.org/aip/apl/article-pdf/doi/10.1063/1.3645633/14459647/143303_1_online.pdf.

[41]P. G. Savvidis, L. G. Connolly, M. S. Skolnick, D. G. Lidzey, and J. J. Baumberg, "Ultrafast polariton dynamics in strongly coupled zinc porphyrin microcavities at room temperature," Phys. Rev. B **74**, 113312 (2006).

[42]S. T. Wanasinghe, A. Gjoni, W. Burson, C. Majeski, B. Zaslona, and A. S. Rury, "Motional narrowing through photonic exchange: Rational suppression of excitonic disorder from molecular cavity polariton formation," J. Phys. Chem. Lett. **15**, 2405–2418 (2024).

[43]W. Ying, M. E. Mondal, and P. Huo, "Theory and quantum dynamics simulations of exciton-polariton motional narrowing," J. Chem. Phys. **161**, 064105 (2024).

[44]J. Dong, Y. Wang, R. Wang, L. Wang, J. Wang, Y. Zhang, Y. Wang, X. Wang, S. Shen, and H. Zhu, "Low-threshold colloidal quantum dots polariton lasing via a strong coupling microcavity at room temperature," Nanoscale (2025), 10.1039/D4NR05185H.

[45]M. Amin, E. R. Koessler, O. Morshed, F. Awan, N. M. B. Cogan, R. Collison, T. M. Tumiel, W. Girten, C. Leiter, A. N. Vamivakas, P. Huo, and T. D. Krauss, "Cavity controlled upconversion in cdse nanoplatelet polaritons," ACS Nano **18**, 21388–21398 (2024), pMID: 39078943, https://doi.org/10.1021/acsnano.4c05871.

[46]Y. A. G. Jomaso, B. Vargas, D. L. Domínguez, R. J. Armenta-Rico, H. E. Sauceda, C. L. Ordoñez-Romero, H. A. Lara-García, A. Camacho-Guardian, and G. Pirruccio, "Intercavity polariton slows down dynamics in strongly coupled cavities," Nat. Commun. **15**, 2915 (2024).

[47]J. Huang, W. Liu, M. C. Sarihan, X. Cheng, A. Miranda, B. Dwir, A. Rudra, E. Kapon, and C. W. Wong, "Exciton-polariton dynamics of the single site-controlled quantum dot-nanocavity in the coexisting strong-weak coupling regime," New J. Phys. **25**, 033015 (2023).

[48]Z. Zhang, P. Saurabh, K. E. Dorfman, A. Debnath, and S. Mukamel, "Monitoring polariton dynamics in the lhcii photosynthetic antenna in a microcavity by two-photon coincidence counting," J. Chem. Phys. **148**, 074302 (2018), https://pubs.aip.org/aip/jcp/article-pdf/doi/10.1063/1.5004432/14899137/074302_1_online.pdf.

[49]T. Khazanov, S. Gunasekaran, A. George, R. Lomlu, S. Mukherjee, and A. J. Musser, "Embrace the darkness: An experimental perspective on organic exciton–polaritons," Chem. Phys. Rev. **4**, 041305 (2023), https://pubs.aip.org/aip/cpr/article-pdf/doi/10.1063/5.0168948/18207413/041305_1_5.0168948.pdf.
[50]E. Michail, K. Rashidi, B. Liu, G. He, V. M. Menon, and M. Y. Sfeir, "Addressing the dark state problem in strongly coupled organic exciton-polariton systems," Nano Lett. **24**, 557–565 (2024), pMID: 38179964, https://doi.org/10.1021/acs.nanolett.3c02984.
[51]M. Laitz, A. E. K. Kaplan, J. Deschamps, U. Barotov, A. H. Proppe, I. García-Benito, A. Osherov, G. Grancini, D. W. deQuilettes, K. A. Nelson, M. G. Bawendi, and V. Bulović, "Uncovering temperature-dependent exciton-polariton relaxation mechanisms in hybrid organic-inorganic perovskites," Nat. Commun. **14**, 2426 (2023).
[52]B. Liu, V. M. Menon, and M. Y. Sfeir, "The role of long-lived excitons in the dynamics of strongly coupled molecular polaritons," ACS Photonics **7**, 2292–2301 (2020), https://doi.org/10.1021/acsphotonics.0c00895.
[53]J. Mony, M. Hertzog, K. Kushwaha, and K. Börjesson, "Angle-independent polariton emission lifetime shown by perylene hybridized to the vacuum field inside a fabry–pérot cavity," J. Phys. Chem. C **122**, 24917–24923 (2018).
[54]B. Xiang, R. F. Ribeiro, L. Chen, J. Wang, M. Du, J. Yuen-Zhou, and W. Xiong, "State-selective polariton to dark state relaxation dynamics," J. Phys. Chem. A **123**, 5918–5927 (2019), pMID: 31268708.
[55]J. Larson and T. Mavrogordatos, ***The Jaynes–Cummings Model and Its Descendants***, 2053-2563 (IOP Publishing, 2021).
[56]J. Knoester and S. Mukamel, "Intermolecular forces, spontaneous emission, and superradiance in a dielectric medium: Polariton-mediated interactions," Phys. Rev. A **40**, 7065–7080 (1989).
[57]R. H. Dicke, "Coherence in spontaneous radiation processes," Phys. Rev. **93**, 99–110 (1954).
[58]Z. Zhou, H.-T. Chen, J. E. Subotnik, and A. Nitzan, "Interplay between disorder, local relaxation, and collective behavior for an ensemble of emitters outside versus inside a cavity," Phys. Rev. A **108**, 023708 (2023).
[59]H.-T. Chen, Z. Zhou, M. Sukharev, J. E. Subotnik, and A. Nitzan, "Interplay between disorder and collective coherent response: Superradiance and spectral motional narrowing in the time domain," Phys. Rev. A **106**, 053703 (2022).
[60]M.-W. Lee, Y.-T. Chuang, and L.-Y. Hsu, "Theory of molecular emission power spectra. ii. angle, frequency, and distance dependence of electromagnetic environment factor of a molecular emitter in plasmonic environments," J. Chem. Phys. **155**, 074101 (2021), https://pubs.aip.org/aip/jcp/article-pdf/doi/10.1063/5.0057018/13634824/074101_1_online.pdf.
[61]S. Wang, M.-W. Lee, Y.-T. Chuang, G. D. Scholes, and L.-Y. Hsu, "Theory of molecular emission power spectra. i. macroscopic quantum electrodynamics formalism," J. Chem. Phys. **153**, 184102 (2020), https://pubs.aip.org/aip/jcp/article-pdf/doi/10.1063/5.0027796/15580598/184102_1_online.pdf.
[62]F. Herrera and F. C. Spano, "Theory of nanoscale organic cavities: The essential role of vibration-photon dressed states," ACS Photonics **5**, 65–79 (2018).
[63]M. Sukharev and A. Nitzan, "Optics of exciton-plasmon nanomaterials," J. Phys.-Condens. Mat. **29**, 443003 (2017).
[64]R. Houdré, R. P. Stanley, and M. Ilegems, "Vacuum-field rabi splitting in the presence of inhomogeneous broadening: Resolution of a homogeneous linewidth in an inhomogeneously broadened system," Phys. Rev. A **53**, 2711–2715 (1996).
[65]B. Renaud, R. M. Whitley, and C. R. S. Jr, "Nonstationary two-level resonance fluorescence," J. Phys. B-At. Mol. Opt. **10**, 19 (1977).
[66]J. B. Pérez-Sánchez, A. Koner, S. Raghavan-Chitra, and J. Yuen-Zhou, "Cut-e as a 1/ ¡i¿n¡/i¿ expansion for multiscale molecular polariton dynamics," J. Chem. Phys. **162** (2025), 10.1063/5.0244452.
[67]J. B. Pérez-Sánchez, F. Mellini, N. C. Giebink, and J. Yuen-Zhou, "Collective polaritonic effects on chemical dynamics suppressed by disorder," Phys. Rev. Research **6**, 013222 (2024).
[68]J. B. Pérez-Sánchez, A. Koner, N. P. Stern, and J. Yuen-Zhou, "Simulating molecular polaritons in the collective regime using few-molecule models," Proc. Natl. Acad. Sci. USA **120** (2023), 10.1073/pnas.2219223120.
[69]M. E. Mondal, A. N. Vamivakas, S. T. Cundiff, T. D. Krauss, and P. Huo, "Polariton spectra under the collective coupling regime. i. efficient simulation of linear spectra and quantum dynamics," J. Chem. Phys. **162** (2025), 10.1063/5.0243535.
[70]M. E. Mondal, A. N. Vamivakas, S. T. Cundiff, T. D. Krauss, and P. Huo, "Polariton spectra under the collective coupling regime. ii. 2d non-linear spectra," J. Chem. Phys. **162** (2025), 10.1063/5.0249705.
[71]B. X. K. Chng, M. E. Mondal, W. Ying, and P. Huo, "Quantum dynamics simulations of exciton polariton transport," Nano Lett. **25**, 1617–1622 (2025).
[72]Y. Lai, W. Ying, and P. Huo, "Non-equilibrium rate theory for polariton relaxation dynamics," J. Chem. Phys. **161**, 104109 (2024), https://pubs.aip.org/aip/jcp/article-pdf/doi/10.1063/5.0231396/20155900/104109_1_5.0231396.pdf.
[73]F. Herrera and F. C. Spano, "Cavity-controlled chemistry in molecular ensembles," Phys. Rev. Lett. **116**, 238301 (2016).
[74]F. Herrera and F. C. Spano, "Dark vibronic polaritons and the spectroscopy of organic microcavities," Phys. Rev. Lett. **118**, 223601 (2017).
[75]L. Qiu, A. Mandal, O. Morshed, M. T. Meidenbauer, W. Girten, P. Huo, A. N. Vamivakas, and T. D. Krauss, "Molecular polaritons generated from strong coupling between cdse nanoplatelets and a dielectric optical cavity," J. Phys. Chem. Lett. **12**, 5030–5038 (2021).
[76]T. E. Li, B. Cui, J. E. Subotnik, and A. Nitzan, "Molecular polaritonics: Chemical dynamics under strong light–matter coupling," Annu. Rev. Phys. Chem. **73**, 43–71 (2022).
[77]A. Thomas, A. Jayachandran, L. Lethuillier-Karl, R. M. Vergauwe, K. Nagarajan, E. Devaux, C. Genet, J. Moran, and T. W. Ebbesen, "Ground state chemistry under vibrational strong coupling: dependence of thermodynamic parameters on the rabi splitting energy," Nanophotonics **9**, 249–255 (2020).
[78]J. A. Campos-Gonzalez-Angulo, R. F. Ribeiro, and J. Yuen-Zhou, "Resonant catalysis of thermally activated chemical reactions with vibrational polaritons," Nat. Commun. **10**, 4685 (2019).
[79]J. del Pino, J. Feist, and F. J. Garcia-Vidal, "Quantum theory of collective strong coupling of molecular vibrations with a microcavity mode," New J. Phys. **17**, 053040 (2015).
[80]W. Xiong, T. Liu, G. Yin, and H. Bhakta, "The role of delocalization and the number of dark modes in polaritonic systems," Presented at APS March Meeting 2025, Denver, CO, March 17 (2025).
[81]L. P. Lindoy, A. Mandal, and D. R. Reichman, "Investigating the collective nature of cavity-modified chemical kinetics under vibrational strong coupling," Nanophotonics **13**, 2617–2633 (2024).
[82]A. Caldeira and A. Leggett, "Quantum tunnelling in a dissipative system," Ann. Phys. **149**, 374–456 (1983).
[83]M. Tavis and F. W. Cummings, "Approximate solutions for an n-molecule-radiation-field hamiltonian," Phys. Rev. **188**, 692–695 (1969).
[84]M. E. Mondal, E. R. Koessler, J. Provazza, A. N. Vamivakas, S. T. Cundiff, T. D. Krauss, and P. Huo, "Quantum dynamics simulations of the 2d spectroscopy for exciton polaritons," J. Chem. Phys. **159** (2023).
[85]X. Sun and E. Geva, "Non-Condon equilibrium Fermi's golden rule electronic transition rate constants via the linearized semiclassical method," J. Chem. Phys. **144**, 244105 (2016).
[86]Y. Lai and E. Geva, "On simulating the dynamics of elec-

tronic populations and coherences via quantum master equations based on treating off-diagonal electronic coupling terms as a small perturbation," J. Chem. Phys. **155**, 204101 (2021).
[87]H.-P. Breuer and F. Petruccione, ***The Theory of Open Quantum Systems*** (Clarendon, Oxford, 2007).
[88]X. Sun and E. Geva, "Non-Condon nonequilibrium Fermi's golden rule rates from the linearized semiclassical method," J. Chem. Phys. **145**, 064109 (2016).
[89]G. D. Scholes, C. A. DelPo, and B. Kudisch, "Entropy reorders polariton states," J. Phys. Chem. Lett. **11**, 6389–6395 (2020), pMID: 32678609.
[90]E. R. Koessler, A. Mandal, and P. Huo, "Incorporating lindblad decay dynamics into mixed quantum-classical simulations," J. Chem. Phys. **157**, 064101 (2022).
[91]A. S. Sheremet, M. I. Petrov, I. V. Iorsh, A. V. Poshakinskiy, and A. N. Poddubny, "Waveguide quantum electrodynamics: Collective radiance and photon-photon correlations," Rev. Mod. Phys. **95**, 015002 (2023).
[92]V. M. Agranovich, D. M. Basko, and O. A. Dubovsky, "Superradiance of polaritons: Crossover from two-dimensional to three-dimensional crystals," J. Chem. Phys. **106**, 3896–3907 (1997).
[93]S. Wang and L.-Y. Hsu, "Exploring superradiance effects of molecular emitters coupled with cavity photons and plasmon polaritons: A perspective from macroscopic quantum electrodynamics," J. Phys. Chem. C **127**, 12904–12912 (2023).
[94]H. M. Gibbs, G. Khitrova, and S. W. Koch, "Exciton–polariton light–semiconductor coupling effects," Nat. Photonics **5**, 273–273 (2011).
[95]P. Michetti and G. C. L. Rocca, "Exciton-phonon scattering and photoexcitation dynamics in j-aggregate microcavities," Phys. Rev. B **79** (2009), 10.1103/PhysRevB.79.035325.
[96]M. Takahata, K. Tanaka, and N. Naka, "Superradiance-to-polariton crossover of wannier excitons with multiple resonances," Phys. Rev. Lett. **121**, 173604 (2018).
[97]H. Zoubi and H. Ritsch, "Superradiant and dark exciton states in an optical lattice within a cavity," Europhys. Lett. **87**, 23001 (2009).
[98]K. Schwennicke, N. C. Giebink, and J. Yuen-Zhou, "Extracting accurate light–matter couplings from disordered polaritons," Nanophotonics **13**, 2469–2478 (2024).
[99]T. Gera and K. L. Sebastian, "Effects of disorder on polaritonic and dark states in a cavity using the disordered tavis–cummings model," J. Chem. Phys. **156** (2022), 10.1063/5.0086027.
[100]T. Gera and K. L. Sebastian, "Exact results for the tavis-cummings and hückel hamiltonians with diagonal disorder," J. Phys. Chem. A **126**, 5449–5457 (2022).
[101]K. Sun, C. Dou, M. F. Gelin, and Y. Zhao, "Dynamics of disordered tavis–cummings and holstein–tavis–cummings models," J. Chem. Phys. **156** (2022), 10.1063/5.0076485.
[102]T. Liu, G. Yin, and W. Xiong, "Unlocking delocalization: how much coupling strength is required to overcome energy disorder in molecular polaritons?" Chem. Sci. **16**, 4676–4683 (2025).
[103]R. H. Tichauer, J. Feist, and G. Groenhof, "Multi-scale dynamics simulations of molecular polaritons: The effect of multiple cavity modes on polariton relaxation," J. Chem. Phys. **154**, 104112 (2021).
[104]T. E. Li, "Vibrational polaritons with broken in-plane translational symmetry," J. Chem. Phys. **161** (2024), 10.1063/5.0209212.
[105]B. X. K. Chng, M. E. Mondal, W. Ying, and P. Huo, "Quantum dynamics simulations of exciton polariton transport," **25**, 1617–1622 (2025).
[106]W. Ying, B. X. K. Chng, M. Delor, and P. Huo, "Microscopic theory of polariton group velocity renormalization," Nat. Commun. **16**, 6950 (2025).